Cell Reports
Medicine

Article

Longitudinal analysis of humoral immunity against SARS-CoV-2 Spike in convalescent individuals up to 8 months post-symptom onset

Graphical abstract

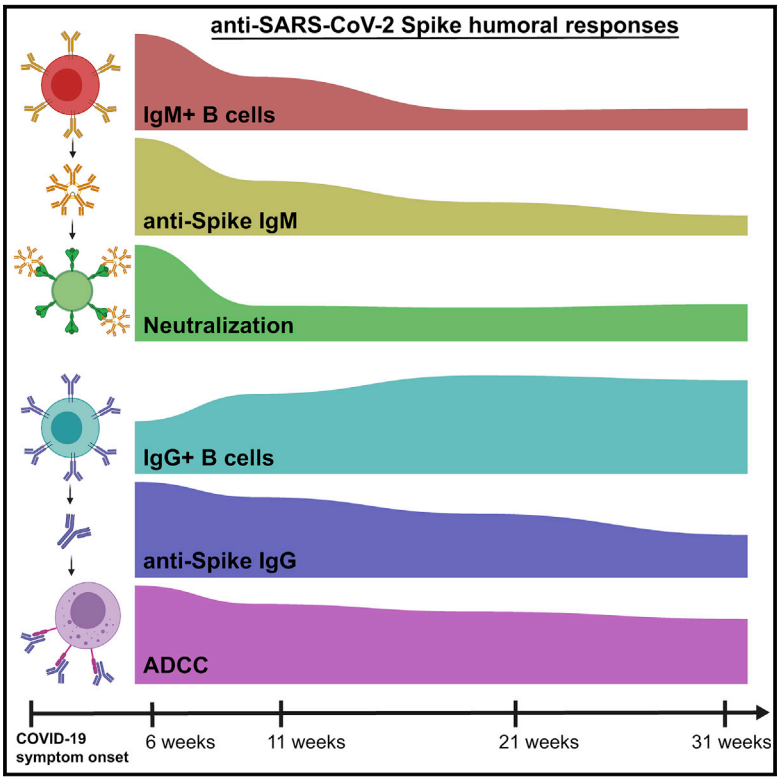

Highlights

- Spike-specific IgM and IgA wane more rapidly than IgG after recovery
- Fc-effector functions, but not neutralization, are sustained over time
- SARS-CoV-2-specific B cell immunity persists despite overall antibody decline

Authors

Sai Priya Anand, Jérémie Prévost, Manon Nayrac, ..., Ralf Duerr, Daniel E. Kaufmann, Andrés Finzi

Correspondence

ralf.duerr@nyulangone.org (R.D.), daniel.kaufmann@umontreal.ca (D.E.K.), andres.finzi@umontreal.ca (A.F.)

In brief

In a cohort of SARS-CoV-2-recovered individuals, Anand et al. observe a concomitant decrease of IgM and neutralization although IgG and Fc-effector functions remain relatively stable. The presence and persistence of antigen-specific memory B cells in all individuals are encouraging with regards to long-term immunity.

Anand et al., 2021, Cell Reports Medicine 2, 100290
June 15, 2021
https://doi.org/10.1016/j.xcrm.2021.100290

CellPress

Cell Reports Medicine

CellPress
OPEN ACCESS

Article

Longitudinal analysis of humoral immunity against SARS-CoV-2 Spike in convalescent individuals up to 8 months post-symptom onset

Sai Priya Anand,[1,2,8] Jérémie Prévost,[2,3,8] Manon Nayrac,[2,3,8] Guillaume Beaudoin-Bussières,[2,3,8] Mehdi Benlarbi,[2] Romain Gasser,[2,3] Nathalie Brassard,[2] Annemarie Laumaea,[2,3] Shang Yu Gong,[1,2] Catherine Bourassa,[2] Elsa Brunet-Ratnasingham,[2,3] Halima Medjahed,[2] Gabrielle Gendron-Lepage,[2] Guillaume Goyette,[2] Laurie Gokool,[2] Chantal Morrisseau,[2] Philippe Bégin,[2,5] Valérie Martel-Laferrière,[2,3] Cécile Tremblay,[2,3] Jonathan Richard,[2,3] Renée Bazin,[4] Ralf Duerr,[6,*] Daniel E. Kaufmann,[2,7,*] and Andrés Finzi[1,2,3,9,*]

[1]Department of Microbiology and Immunology, McGill University, Montreal, QC H3A 2B4, Canada
[2]Centre de Recherche du CHUM, Montreal, QC H2X 0A9, Canada
[3]Département de Microbiologie, Infectiologie et Immunologie, Université de Montréal, Montreal, QC H2X 0A9, Canada
[4]Héma-Québec, Affaires Médicales et Innovation, Quebec, QC G1V 5C3, Canada
[5]CHU Ste-Justine, Montreal, QC H3T 1C5, Canada
[6]Departments of Pathology and Microbiology, New York University School of Medicine, New York, NY 10016, USA
[7]Département de Médecine, Université de Montréal, Montreal, QC H3T 1J4, Canada
[8]These authors contributed equally
[9]Lead contact
*Correspondence: ralf.duerr@nyulangone.org (R.D.), daniel.kaufmann@umontreal.ca (D.E.K.), andres.finzi@umontreal.ca (A.F.)
https://doi.org/10.1016/j.xcrm.2021.100290

SUMMARY

With the recent approval of highly effective coronavirus disease 2019 (COVID-19) vaccines, functional and lasting immunity to severe acute respiratory syndrome coronavirus 2 (SARS-CoV-2) is currently under investigation as antibody levels in plasma were shown to decline during convalescence. Since the absence of antibodies does not equate to absence of immune memory, we evaluate the presence of SARS-CoV-2-specific memory B cells in convalescent individuals. Here, we report a longitudinal assessment of humoral immune responses on 32 donors up to 8 months post-symptom onset. Our observations indicate that anti-Spike and anti-receptor binding domain (RBD) immunoglobulin M (IgM) in plasma decay rapidly, whereas the reduction of IgG is less prominent. Neutralizing activity also declines rapidly when compared to Fc-effector functions. Concomitantly, the frequencies of RBD-specific IgM+ B cells wane significantly when compared to RBD-specific IgG+ B cells, which remain stable. Our results add to the current understanding of immune memory following SARS-CoV-2 infection, which is critical for secondary infection prevention and vaccine efficacy.

INTRODUCTION

Severe acute respiratory syndrome coronavirus 2 (SARS-CoV-2), the causative agent of the ongoing coronavirus disease 2019 (COVID-19) pandemic, is highly contagious and has infected close to a 100 million people worldwide and caused over 2 million deaths since its discovery. The dynamics and persistence of immune responses in individuals infected with SARS-CoV-2 is currently under needful investigation. Several studies with acute and convalescent COVID-19 patients have showed prompt induction of B and T cell responses upon infection, along with the detection of antigen-specific memory B and T cell responses several weeks into convalescence.[1–6] Additionally, antibodies (Abs) induced upon infection have been shown to protect from SARS-CoV-2 reinfection in animal models.[7–9] Passive immunization using neutralizing monoclonal antibody treatments decreased viral loads in animal studies and in patients with COVID-19.[10,11] The viral target of neutralizing antibodies is the highly immunogenic trimeric Spike (S) glycoprotein, which facilitates SARS-CoV-2 entry into host cells via its receptor-binding domain (RBD) that interacts with angiotensin-converting enzyme 2 (ACE-2).[12,13]

The evolution of overall antibody responses in convalescent individuals is being extensively analyzed, with studies showing that Ab titers and neutralization activity against Spike start decreasing during the first weeks after resolution of infection.[3,6,14–20] Importantly, in addition to neutralizing viral particles, the antiviral activities of SARS-CoV-2-specific antibodies can expand to involve Fc-effector functions, including antibody-dependent cellular cytotoxicity (ADCC).[21,22] Recent research has highlighted the importance of humoral immunity development and the ability of antibodies to carry out Fc-effector functions in decreasing mortality of patients exhibiting severe disease symptoms.[23]

Table 1. Longitudinal SARS-CoV-2 convalescent cohort

Group	N	Days after onset of symptoms (median; day range)	Age (median; age range)	Gender	
				Male (n)	Female (n)
6 weeks	32	43 (16–95)	47 (20–65)	17	15
11 weeks	28	77 (48–127)	47 (20–65)	16	12
21 weeks	28	145 (116–171)	48 (20–65)	16	12
31 weeks	13	218 (201–233)	46 (20–65)	9	4

In this study, we dissect multiple aspects of humoral immunity, including Fc-effector functions and antigen-specific B cells, longitudinally for up to 8 months post-symptom onset (PSO) in 32 convalescent individuals. Our findings aid in the understanding of durability of COVID-19 immunity, which is important in the context of secondary infections, vaccine efficacy, and herd immunity.

RESULTS

SARS-CoV-2 RBD-specific and Spike-specific antibody levels in convalescent plasma decrease up to 8 months PSO

To monitor the evolution of antibody responses longitudinally, we analyzed serological samples from 32 convalescent individuals (Table 1) along with 10 pre-pandemic samples from uninfected individuals as experimental controls. The average age of the donors was 47 years old (range: 20–65 years), and samples were from 17 males and 15 females. Convalescent patients were sampled at four longitudinal time points between 16 and 233 days PSO: 6 weeks (16–95 days; median: 43 days); 11 weeks (48–127 days; median: 77 days); 21 weeks (116–171 days; median: 145 days); and 31 weeks (201–233 days; median: 218 days). Participants were tested positive for SARS-CoV-2 infection by reverse transcription PCR (RT-PCR) on nasopharyngeal swab specimens, had mild to moderate disease symptoms, and none of them were hospitalized. Convalescent participants were enrolled following two negative RT-PCR tests and a complete resolution of symptoms for at least 14 days before blood sampling.

We began by evaluating the presence of RBD-specific antibodies by using a previously published enzyme-linked immunosorbent assay (ELISA) against the SARS-CoV-2 RBD antigen.[16] In agreement with recent reports showing the waning of antibody levels in longitudinal convalescent plasma over time,[14–17] we observed that total RBD-specific immunoglobulin (Ig) levels, comprising IgG, IgM, and IgA, gradually decreased between 6 and 31 weeks after the onset of symptoms (Figure 1A). However, the percentage of convalescent individuals presenting detectable RBD-specific Ig levels remained stable, with a consistent seropositivity rate above 90% throughout the sampling time frame. Notably, 100% of the donors still had detectable IgG at the last time point, while IgM and IgA diminished more rapidly, with 85% and 69% of the donors having undetectable IgM and IgA levels, respectively, 31 weeks PSO (Figures 1B–1D and S1A). Because the RBD ELISA is limited to detect antibodies targeting only one domain of the Spike, we developed a high-throughput cell-based ELISA methodology to screen for antibodies recognizing the native full-length S protein on the cell surface. Human osteosarcoma (HOS) cells stably expressing the SARS-CoV-2 S glycoproteins were incubated with plasma samples, followed by the addition of secondary antibodies recognizing IgG, IgM, and/or IgA. We observed that 100% of the donors still had detectable S-specific total Ig and IgG in their plasma at 31 weeks PSO, whereas only 38% and 54% of the plasma samples tested positive for the presence of Spike-specific IgM and IgA, respectively (Figures 1E–1H and S1B). We confirmed this observation using a recently characterized flow-cytometry-based assay[24] determining antibody binding to the full-length S protein on the surface of 293T cells (Figure S2A). The data obtained with both the cell-based ELISA and flow-cytometry techniques correlated significantly ($r = 0.8120$; $p < 0.0001$; Figure S2B).

Neutralizing and Fc-effector activities of antibodies present in convalescent plasma decrease at different rates over time

Recent studies have shown the importance of neutralizing antibodies in reducing viral load and preventing infection in animal models.[10,25,26] Neutralizing monoclonal antibody cocktails also reduced viral load in COVID-19 patients.[11] Neutralizing activity is often considered as a determining factor in convalescent plasma therapy, although its relative importance compared to Fc-effector activity is still unknown.[27–29] Thus, we measured the capacity of convalescent plasma to neutralize pseudoviral particles carrying the SARS-CoV-2 Spike protein over time. Neutralizing antibody titers (inhibitory dilution [ID_{50}]) were detected in 63% of the donors at 6 weeks PSO, while none of the uninfected controls had detectable neutralizing activity. Titers declined from 155.6 at 6 weeks to 60.0 at 31 weeks PSO, respectively, with 77% of donors having undetectable neutralization activity in their plasma at the last time point (Figure 2A). Of note, plasma from individuals that had undetectable neutralization activity at later time points started with lower peak titers at earlier time points. Because the depletion of IgM from plasma has been associated with loss of viral neutralization capacity[30,31] and IgA has also been shown to dominate the early neutralizing response,[32,33] the sharp decline in neutralization activity seen in this study is corroborated by the striking decrease in anti-Spike and anti-RBD IgM and IgA levels (Figures 1B, 1D, 1F, 1H, S1A, S1B, and S5).

Fc-mediated effector functions of antibodies can contribute to the efficacy of immune response against SARS-CoV-2. Recent studies have examined Fc-mediated effector functions of antibodies elicited upon SARS-CoV-2 infection.[21,34,35] Both the presence of IgG and their Fc-mediated effector activities have been linked to reduced severity of disease.[23] Herein, we assessed the ability of plasma from convalescent donors to trigger ADCC responses over time. We developed an ADCC assay using a human T-lymphoid cell line resistant to NK-cell-mediated cell lysis (CEM.NKr) and stably expressing the full-length S protein on the cell surface as target cells. Peripheral blood mononuclear cells (PBMCs) from healthy individuals were used as effector cells. ADCC activity was measured by the loss of

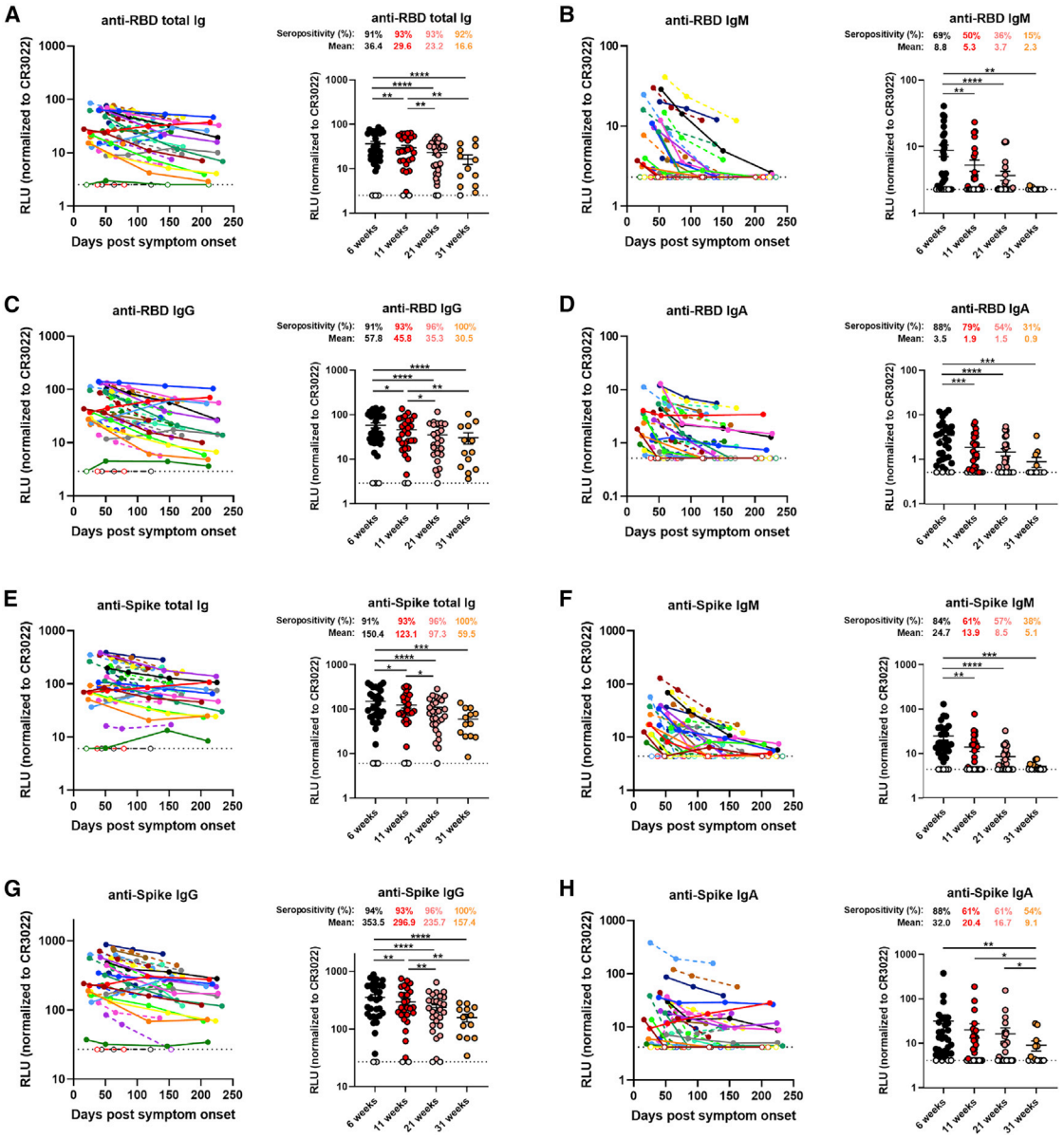

Figure 1. Decline of RBD- and Spike-specific antibodies in longitudinal convalescent plasma

(A–D) Indirect ELISA was performed using recombinant SARS-CoV-2 RBD protein and incubation with COVID-19+ plasma samples recovered between 6 and 31 weeks post-symptom onset. Anti-RBD antibody binding was detected using horseradish peroxidase (HRP)-conjugated (A) anti-human IgM+IgG+IgA, (B) anti-human IgM, (C) anti-human IgG, or (D) anti-human IgA. Relative light unit (RLU) values obtained with BSA (negative control) were subtracted and further normalized to the signal obtained with the anti-RBD CR3022 monoclonal antibody (mAb) present in each plate.

(E–H) Cell-based ELISA was performed using HOS cells expressing full-length SARS-CoV-2 Spike and incubation with COVID-19+ plasma samples recovered between 6 and 31 weeks post-symptom onset. Anti-Spike antibody binding was detected using HRP-conjugated (E) anti-human IgM+IgG+IgA, (F) anti-human IgM, (G) anti-human IgG, or (H) anti-human IgA. RLU values obtained with parental HOS (negative control) were subtracted and further normalized to the signal obtained with the CR3022 mAb present in each plate.

(Left panels) Each curve represents the normalized RLUs obtained with the plasma of one donor at every donation as a function of the days after symptom onset. (Right panels) Plasma samples were grouped in different time points post-symptom onset (6, 11, 21, and 31 weeks). Undetectable measures are represented as white symbols, and limits of detection are plotted. Error bars indicate means ± SEM. Statistical significance was tested using repeated-measures one-way ANOVA with a Holm-Sidak post-test (*$p < 0.05$; **$p < 0.01$; ***$p < 0.001$; ****$p < 0.0001$).

Spike-expressing GFP+ target cells (Figure S3). We observed that ADCC activity of convalescent plasma decreased gradually between 6 weeks and 31 weeks PSO (Figure 2B). However, this decline was modest when compared to the decrease in neutralization activity of plasma (Figure S1C), and 85% of the donors' plasma still elicited substantial ADCC activity at the latest study

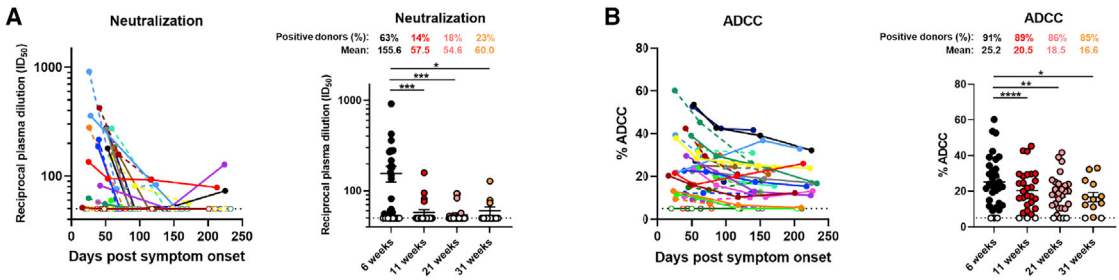

Figure 2. Neutralization and Fc-effector function activities in convalescent plasma decrease over time

(A) Pseudoviral particles coding for the luciferase reporter gene and bearing the SARS-CoV-2 S glycoproteins were used to infect 293T-ACE2 cells. Neutralizing activity was measured by incubating pseudoviruses with serial dilutions of COVID-19+ plasma samples recovered between 6 and 31 weeks post-symptom onset at 37°C for 1 h prior to infection of 293T-ACE2 cells. Neutralization half-maximal inhibitory serum dilution (ID_{50}) values were determined using a normalized non-linear regression using GraphPad Prism software.

(B) CEM.NKr parental cells were mixed at a 1:1 ratio with CEM.NKr-Spike cells and were used as target cells. PBMCs from uninfected donors were used as effector cells in a fluorescence-activated cell sorting (FACS)-based ADCC assay. The graphs shown represent the percentages of ADCC obtained in the presence of COVID-19+ plasma samples recovered between 6 and 31 weeks post-symptom onset.

(Left panels) Each curve represents (A) the neutralization ID_{50} or (B) the percentages of ADCC obtained with the plasma of one donor at every donation as a function of the days after symptom onset. (Right panels) Plasma samples were grouped in different time points post-symptom onset (6, 11, 21, and 31 weeks). Undetectable measures are represented as white symbols, and limits of detection are plotted. Error bars indicate means ± SEM. Statistical significance was tested using repeated-measures one-way ANOVA with a Holm-Sidak post-test (*$p < 0.05$; **$p < 0.01$; ***$p < 0.001$; ****$p < 0.0001$).

time point. As expected, the levels of ADCC activity strongly correlated with the levels of anti-Spike IgG (Figure S5). The presence of Fc-mediated antibody effector functions up to 8 months PSO is corroborated with the presence of significant IgG levels.

RBD-specific memory B cells develop and remain stable up to 8 months PSO

Recent studies on convalescent COVID-19 patients have indicated persistent antigen-specific memory B cell responses despite waning antibody levels.[3,6] To monitor the circulating B cell compartment in our cohort of convalescent individuals, antigen-specific B cells were characterized by flow cytometry (identified as CD19+ CD20+). We focused on RBD-specific B cell responses to avoid selecting for pre-existing memory B cells cross-reactive with endemic coronaviruses.[36] To identify distinct RBD-specific B cells, we used double discrimination with two recombinant RBD protein preparations labeled with fluorochromes Alexa Fluor 594 and Alexa Fluor 488, respectively. Detection of this double-positive population was specific because it was not detected in PBMCs from uninfected individuals (Figures S4A and S4B). RBD-specific B cells were detected 6 weeks PSO with a modest increase in mean frequency up to 31 weeks PSO (0.038%–0.051%; Figure 3B). Total RBD-specific B cells were evaluated for their differential surface Ig isotype expression, and we observed IgG+, IgM+, and IgA+ cells in 100%, 92%, and 83% of donors at 6 weeks PSO, respectively. Strikingly, the frequency of RBD-specific IgM+ B cells decreased significantly, with 46% of the donors having undetectable IgM+ B cells 31 weeks PSO (Figures 3C and S1D). Conversely, the frequency of RBD-specific IgG+ B cells significantly increased between 6 and 21 weeks PSO and remained stable up to 8 months PSO (Figure 3D); the detection of RBD-specific IgA+ B cells also persisted in 77% of the donors tested (Figures 3E and S1D). Furthermore, the total RBD-specific B cells were evaluated to distinguish memory and naive B cells (identified by using CD27 and CD21 markers; Figures S4C and S4D). Importantly, total RBD-specific memory B cells were detected in 100% of the donors and the mean frequency remained stable between 6 and 31 weeks PSO (0.020%–0.026%), while RBD-specific naive B cells were observed in lower proportions and modestly decreased over time (Figures 3F and 3G). Interestingly, the proportion of donors positive for RBD-specific naive B cells was reduced by half between the first and last time point, as also observed for RBD-specific IgM+ B cells, which is consistent with the decline in IgM levels observed between these groups. IgG+ RBD-specific memory B cells were detected in 100% of the donors, and the frequency of this population modestly increased up to 31 weeks PSO (Figure 3H). Meanwhile, the frequencies of IgA+ RBD-specific memory B cells were low but stable over the 8-month period (Figures 3G and 3I).

Evaluation of the relationship between different aspects of humoral immunity reveals the importance of IgG responses

To examine interrelations between serological, immunological, and functional parameters assessed in this study, we performed comprehensive sets of correlation analyses. First, at each time point, the strongest immune response clusters were composed of total Ig and IgG binding levels and, thus, increased ADCC activity (Figure 4A, left panel). In contrast, weaker immune response clusters in plasma were formed by IgA and IgM levels and, subsequently, neutralization capacities. Overall, the responses decreased over the course of the 8-month period (Figure 4B). The inverse was observed with antigen-specific B cell frequencies (Figure 4B). Apart from naive B cells and the IgM fraction thereof, total RBD-specific B cells increased over the course of 8 months. At each time point, total IgG+ B cells and memory B cells (IgA+ and IgG+) constituted the most prominent responses (Figure 4A, right panel).

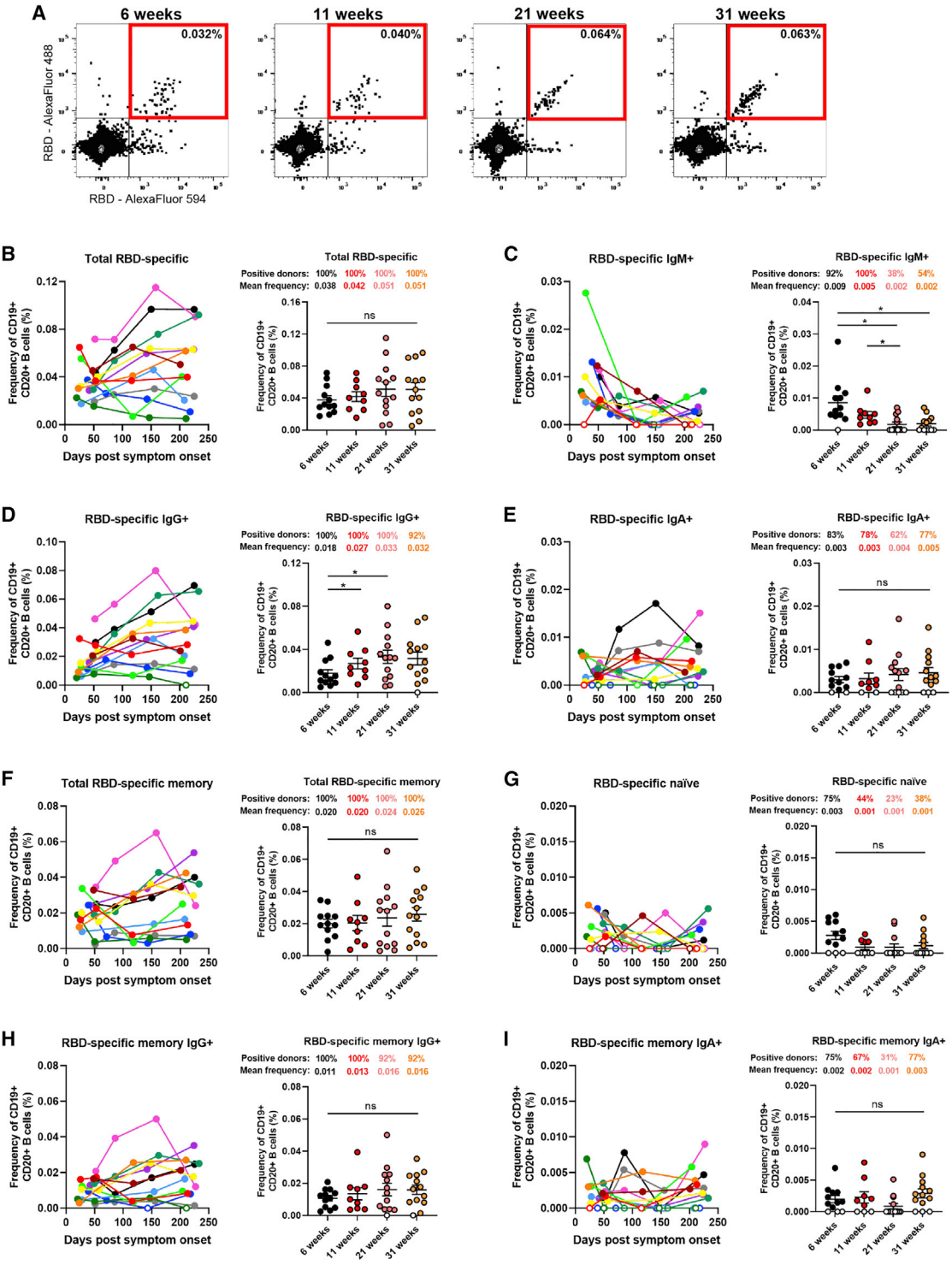

Figure 3. RBD-specific memory B cells develop and persist up to 8 months post-symptom onset

(A) Flow cytometry plots of staining with fluorescent SARS-CoV-2 RBD probes on CD19+ CD20+ HLA-DR+ B cells. Samples from one representative convalescent donor are shown for 4 different time points post-symptom onset (6, 11, 21, and 31 weeks). All percentages shown represent the frequency of RBD-specific B cells on the total CD19+ CD20+ B cell population.

(B–G) Characterization of RBD-specific B cells was performed on longitudinal PBMC samples obtained from COVID-19+ convalescent individuals between 6 and 31 weeks post-symptom onset.

(B–E) Total (B) RBD-specific B cells were segregated by subsets based on cell surface expression of (C) IgM, (D) IgG, or (E) IgA BCR isotypes.

(legend continued on next page)

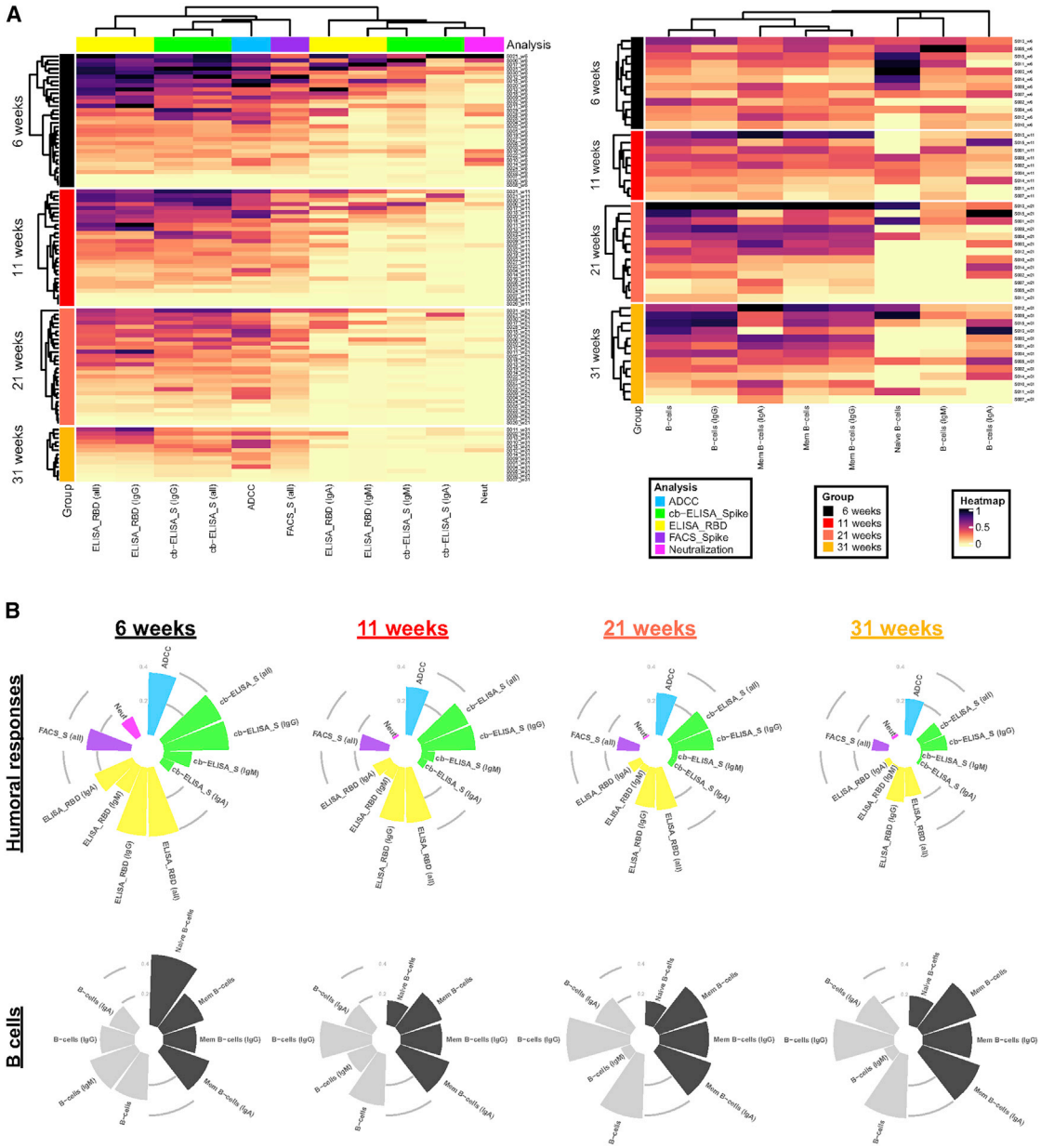

Figure 4. Longitudinal patterns of B cell levels and humoral immune responses

(A) (Left panel) Heatmap of humoral immune responses normalized per parameter. Columns represent immune response parameters clustered based on similarity and grouped according to the provided color code. Rows represent IDs grouped according to study time point. IDs are clustered according to their immune response profiles within each time point. (Right panel) Heatmap of B cell levels with similar display as in left panel is shown.

(B) Circular bar plots represent averaged values of parameters at each time point.

Additionally, at the earliest time point convalescent plasma was collected after symptom onset (6 weeks PSO), we observed a vast network of strong positive correlations among B cell populations, antibody levels, and antibody-mediated functional parameters (Figure 5B). Intriguingly, this was followed by a striking disconnect of associations between B cell frequencies and serological parameters at 11, 21, and 31 weeks PSO (Figures 5C–5E). This is caused by the concomitant diminution of antibody levels

(F–I) Frequency of (F) total memory, (G) naive, (H) IgG+ memory, and (I) IgA+ memory B cells was determined based on CD21 and CD27 expression.

(Left panels) Each curve represents the frequency of a B cell subset on the total B cell population obtained with PBMCs from one donor at every donation as a function of the days after symptom onset. (Right panels) PBMC samples were grouped in different time points post-symptom onset (6, 11, 21, and 31 weeks). Error bars indicate means ± SEM. Statistical significance was tested using repeated-measures one-way ANOVA with a Holm-Sidak post-test (*$p < 0.05$; ns, nonsignificant)

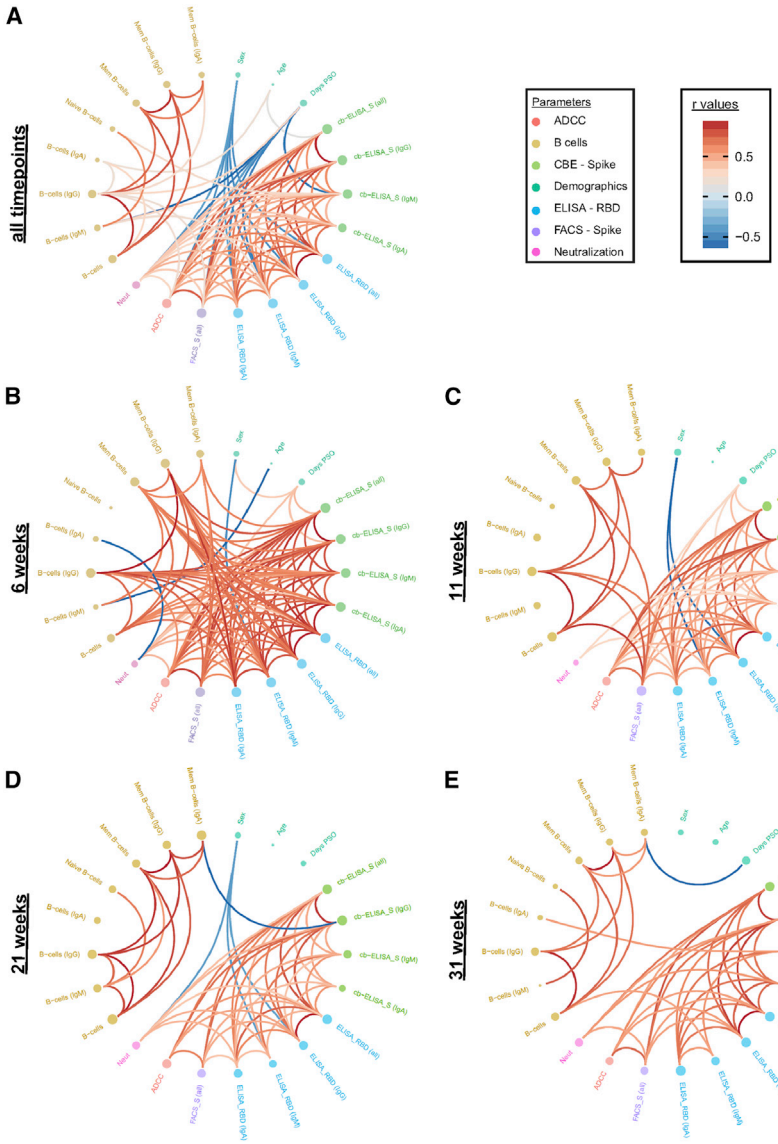

Figure 5. Longitudinal plasticity and separation of B cell and humoral correlation clusters

Edge bundling correlation plots where red and blue edges represent positive and negative correlations between connected parameters, respectively. Only significant correlations ($p < 0.05$) are displayed. Nodes are color coded based on the grouping of parameters according to the legend at the bottom. Node size corresponds to the degree of relatedness of correlations. Edge bundling plots are shown for correlation analyses using all data points (A) and datasets of individual time points, i.e., at 6 weeks (B), 11 weeks (C), 21 weeks (D), and 31 weeks (E).

yet stabilization of antigen-specific B cells observed at these time points, suggestive of decreased antibody production by B cells after resolution of infection or the gradual replacement of Ig-secreting, short-lived plasma cell by memory B cells. When considering the collective datasets, prominent features were two subsequently dividing positive correlation clusters, the first among total and IgG+ RBD-specific B cells and the second among ADCC with total Ig and IgG binding responses. Furthermore, days PSO inversely correlated with neutralization as well as IgM- and IgA-specific responses (Figures 5A and S5).

DISCUSSION

A better understanding of the type and longevity of immune responses following viral infections is critical to reveal immune mechanisms involved in protection from reinfection and protection by vaccination. Data regarding these important issues continue to be gathered for SARS-CoV-2. In this study, we have contributed to the current understanding by reporting on the evolution of the overall humoral immune responses in 101 blood samples obtained from 32 COVID-19 convalescent patients between 16 and 233 days PSO. Overall, we observed that IgM levels and the neutralizing capacity of plasma decreases rapidly, whereas IgG and Fc-effector activity are more sustained. Since disease severity has been shown to correlate with Ig titers and neutralization activity of plasma,[37] the rapid decline of neutralizing activity in our cohort could be linked to the mild severity of symptoms observed by our donors. The antibody kinetics we observed herein are typical of those seen for other human coronavirus infections, with antibodies peaking 2–4 weeks PSO followed by a contraction phase.[38] Furthermore, we show that COVID-19 patients generate RBD-specific memory B cells and IgG+ B memory cells that persist for over 8 months. This is similar to recent studies on the durability of SARS-CoV-2 immune responses showing that, despite decreases in antibody levels, Spike-specific IgG+ memory B cells are generated and maintained likely due to antigen persistence in convalescent individuals.[3,5,6] Additionally, studies demonstrated enhanced cellular immunity that protects non-human primates from SARS-CoV-2 reinfection in the context of waning neutralizing antibodies.[8] Thus, the decline of antibody levels does not negate the protective potential because of the importance of cellular responses against SARS-CoV-2 infection. This understanding is corroborated with a recent risk assessment carried out in a cohort of 43,000 convalescent individuals demonstrating that immunity elicited upon natural SARS-CoV-2 infection protects against reinfection with an efficacy of >90% for at least 7 months.[39]

Fc-mediated effector activity of antibodies has been recently shown to correlate with reduced disease severity and

mortality.[23] Antibodies capable of mediating Fc-dependent functions, such as antibody-dependent phagocytosis and ADCC, have been isolated from convalescent donors.[40] Importantly, Fc-mediated effector activity was shown to contribute to the protection from SARS-CoV-2 infection in adapted mice and hamster models.[9,21,34] Thus, our observations of the persistence of ADCC responses in convalescent plasma up to 8 months PSO suggest that Fc-mediated effector functions could play a vital role in protection from reinfection. Nevertheless, the heterogeneity of immune responses between individuals is and will be an important factor when evaluating the efficacy of immune responses upon re-exposure to SARS-CoV-2.

Recent studies comparing humoral immunity generated by mRNA vaccinees (mRNA-1273 or BNT162b2) and individuals recovered from natural infection observed similarities in antibody binding titers and plasma neutralization capacity.[41] Furthermore, similar frequencies of RBD-specific memory B cells between vaccinees and infected individuals were also detected. Therefore, our results on the persistence of RBD-specific memory B cells up to 8 months after natural infection is reassuring with regards to long-term vaccine efficacy.

Limitations of study

A limitation of the current study is the relatively low number of individuals studied, which can affect the power of our statistical analyses. Longitudinal data from a larger sample size with varying clinical symptoms ranging from asymptomatic to critical cases as well as individuals below 20 years and over 65 years of age would be required for a more precise understanding of the overall immune durability against COVID-19. However, we note that results as obtained in this study are very similar to those observed in larger cross-sectional and longitudinal studies.[3,5,6]

Furthermore, although we successfully used our ADCC assay to show the importance of Fc-mediated effector functions of neutralizing Abs to protect from lethal SARS-CoV-2 challenges in K18-hACE2 transgenic mice[42] and as an immune correlate for survival in acutely infected individuals,[43] our assay uses cells constitutively expressing the Spike proteins and not bona fide SARS-CoV-2-infected cells.

STAR★METHODS

Detailed methods are provided in the online version of this paper and include the following:

- KEY RESOURCES TABLE
- RESOURCE AVAILABILITY
  - Lead contact
  - Materials availability
  - Data and code availability
- EXPERIMENTAL MODEL AND SUBJECT DETAILS
  - Ethics Statement
  - Human subjects
  - Cell lines
- METHOD DETAILS
  - Plasma and antibodies
  - Protein expression and purification
  - Enzyme-Linked Immunosorbent Assay (ELISA)
  - Cell-Based ELISA
  - Cell surface staining and flow cytometry analysis
  - ADCC assay
  - Virus neutralization assay
  - Detection of antigen-specific B cells
- QUANTIFICATION AND STATISTICAL ANALYSIS
  - Statistical analyses
  - Software scripts and visualization

SUPPLEMENTAL INFORMATION

Supplemental information can be found online at https://doi.org/10.1016/j.xcrm.2021.100290.

ACKNOWLEDGMENTS

The authors are grateful to the convalescent plasma donors who participated in this study. The authors thank the CRCHUM BSL3 and Flow Cytometry Platforms for technical assistance. We thank Dr. Stefan Pöhlmann and Dr. Markus Hoffmann (Georg-August University, Germany) for the plasmid coding for SARS-CoV-2 S glycoproteins and Dr. M. Gordon Joyce (US MHRP) for the monoclonal antibody CR3022. The following reagent was obtained through the NIH HIV Reagent Program, Division of AIDS, NIAID, NIH: CEM.NKR CCR5+ Cells, ARP-4376, contributed by Dr. Alexandra Trkola. The graphical abstract was prepared using images from BioRender.com. This work was supported by le Ministère de l'Économie et de l'Innovation du Québec, Programme de soutien aux organismes de recherche et d'innovation to A.F., by the Fondation du CHUM, and by the Fondation du CHU Sainte-Justine. This work was also supported by the American Foundation for AIDS Research (amfAR) to A.F. and D.E.K. This work was also supported by Canada's COVID-19 Immunity Task Force (CITF), in collaboration with the Canadian Institutes of Health Research (CIHR) (grant VR2-173203); a CIHR foundation grant no. 352417 to A.F.; CIHR COVID-19 Rapid Research Funding to A.F., R.B., and P.B.; and by an Exceptional Fund COVID-19 from the Canada Foundation for Innovation (CFI) no. 41027 to A.F. and D.E.K. A.F. is the recipient of Canada Research Chair on Retroviral Entry no. RCHS0235 950-232424. V.M.-L. and P.B. are supported by FRQS Junior 1 salary awards. D.E.K. is a FRQS Merit Research Scholar. R.D. was supported by NIH grant R01 AI122953-05. S.P.A., J.P., and G.B.-B. are supported by CIHR fellowships. R.G. is supported by a MITACS Accélération postdoctoral fellowship. The funders had no role in study design, data collection and analysis, decision to publish, or preparation of the manuscript.

AUTHOR CONTRIBUTIONS

S.P.A., J.P., J.R., and A.F. conceived the study; S.P.A., J.P., M.N., G.B.-B., E.B.-R., J.R., D.E.K., and A.F. designed experimental approaches; S.P.A., J.P., M.N., G.B.-B., M.B., R.G., N.B., A.L., S.Y.G., C.B., G.G.-L., P.B., J.R., R.B., R.D., D.E.K., and A.F. performed, analyzed, and interpreted the experiments; R.D. performed statistical analyses; S.P.A., J.P., J.R., and G.G. contributed novel reagents; A.L., H.M., G.G.-L., L.G., C.M., V.M.-L., and C.T. collected and processed clinical samples; and S.P.A., J.P., R.D., and A.F. wrote the paper. Every author has read, edited, and approved the final manuscript.

DECLARATION OF INTERESTS

The authors declare no competing interests.

Received: January 29, 2021
Revised: March 25, 2021
Accepted: April 27, 2021
Published: May 5, 2021

REFERENCES

1. Rydyznski Moderbacher, C., Ramirez, S.I., Dan, J.M., Grifoni, A., Hastie, K.M., Weiskopf, D., Belanger, S., Abbott, R.K., Kim, C., Choi, J., et al. (2020). Antigen-specific adaptive immunity to SARS-CoV-2 in acute COVID-19 and associations with age and disease severity. Cell *183*, 996–1012.e19.
2. Hartley, G.E., Edwards, E.S.J., Aui, P.M., Varese, N., Stojanovic, S., McMahon, J., Peleg, A.Y., Boo, I., Drummer, H.E., Hogarth, P.M., et al. (2020). Rapid generation of durable B cell memory to SARS-CoV-2 spike and nucleocapsid proteins in COVID-19 and convalescence. Sci. Immunol. *5*, eabf8891.
3. Gaebler, C., Wang, Z., Lorenzi, J.C.C., Muecksch, F., Finkin, S., Tokuyama, M., Cho, A., Jankovic, M., Schaefer-Babajew, D., Oliveira, T.Y., et al. (2021). Evolution of antibody immunity to SARS-CoV-2. Nature *591*, 639–644.
4. Grifoni, A., Weiskopf, D., Ramirez, S.I., Mateus, J., Dan, J.M., Moderbacher, C.R., Rawlings, S.A., Sutherland, A., Premkumar, L., Jadi, R.S., et al. (2020). Targets of T cell responses to SARS-CoV-2 coronavirus in humans with COVID-19 disease and unexposed individuals. Cell *181*, 1489–1501.e15.
5. Dan, J.M., Mateus, J., Kato, Y., Hastie, K.M., Yu, E.D., Faliti, C.E., Grifoni, A., Ramirez, S.I., Haupt, S., Frazier, A., et al. (2021). Immunological memory to SARS-CoV-2 assessed for up to 8 months after infection. Science *371*, eabf4063.
6. Wheatley, A.K., Juno, J.A., Wang, J.J., Selva, K.J., Reynaldi, A., Tan, H.X., Lee, W.S., Wragg, K.M., Kelly, H.G., Esterbauer, R., et al. (2021). Evolution of immune responses to SARS-CoV-2 in mild-moderate COVID-19. Nat. Commun. *12*, 1162.
7. Chandrashekar, A., Liu, J., Martinot, A.J., McMahan, K., Mercado, N.B., Peter, L., Tostanoski, L.H., Yu, J., Maliga, Z., Nekorchuk, M., et al. (2020). SARS-CoV-2 infection protects against rechallenge in rhesus macaques. Science *369*, 812–817.
8. McMahan, K., Yu, J., Mercado, N.B., Loos, C., Tostanoski, L.H., Chandrashekar, A., Liu, J., Peter, L., Atyeo, C., Zhu, A., et al. (2021). Correlates of protection against SARS-CoV-2 in rhesus macaques. Nature *590*, 630–634.
9. Tortorici, M.A., Beltramello, M., Lempp, F.A., Pinto, D., Dang, H.V., Rosen, L.E., McCallum, M., Bowen, J., Minola, A., Jaconi, S., et al. (2020). Ultrapotent human antibodies protect against SARS-CoV-2 challenge via multiple mechanisms. Science *370*, 950–957.
10. Baum, A., Ajithdoss, D., Copin, R., Zhou, A., Lanza, K., Negron, N., Ni, M., Wei, Y., Mohammadi, K., Musser, B., et al. (2020). REGN-COV2 antibodies prevent and treat SARS-CoV-2 infection in rhesus macaques and hamsters. Science *370*, 1110–1115.
11. Weinreich, D.M., Sivapalasingam, S., Norton, T., Ali, S., Gao, H., Bhore, R., Musser, B.J., Soo, Y., Rofail, D., Im, J., et al.; Trial Investigators (2021). REGN-COV2, a neutralizing antibody cocktail, in outpatients with Covid-19. N. Engl. J. Med. *384*, 238–251.
12. Walls, A.C., Park, Y.J., Tortorici, M.A., Wall, A., McGuire, A.T., and Veesler, D. (2020). Structure, function, and antigenicity of the SARS-CoV-2 Spike glycoprotein. Cell *181*, 281–292.e6.
13. Hoffmann, M., Kleine-Weber, H., Schroeder, S., Krüger, N., Herrler, T., Erichsen, S., Schiergens, T.S., Herrler, G., Wu, N.H., Nitsche, A., et al. (2020). SARS-CoV-2 cell entry depends on ACE2 and TMPRSS2 and is blocked by a clinically proven protease inhibitor. Cell *181*, 271–280.e8.
14. Beaudoin-Bussières, G., Laumaea, A., Anand, S.P., Prévost, J., Gasser, R., Goyette, G., Medjahed, H., Perreault, J., Tremblay, T., Lewin, A., et al. (2020). Decline of humoral responses against SARS-CoV-2 Spike in convalescent individuals. MBio *11*, e02590-20.
15. Perreault, J., Tremblay, T., Fournier, M.J., Drouin, M., Beaudoin-Bussières, G., Prévost, J., Lewin, A., Bégin, P., Finzi, A., and Bazin, R. (2020). Waning of SARS-CoV-2 RBD antibodies in longitudinal convalescent plasma samples within 4 months after symptom onset. Blood *136*, 2588–2591.
16. Prévost, J., Gasser, R., Beaudoin-Bussières, G., Richard, J., Duerr, R., Laumaea, A., Anand, S.P., Goyette, G., Benlarbi, M., Ding, S., et al. (2020). Cross-sectional evaluation of humoral responses against SARS-CoV-2 Spike. Cell Rep. Med. *1*, 100126.
17. Robbiani, D.F., Gaebler, C., Muecksch, F., Lorenzi, J.C.C., Wang, Z., Cho, A., Agudelo, M., Barnes, C.O., Gazumyan, A., Finkin, S., et al. (2020). Convergent antibody responses to SARS-CoV-2 in convalescent individuals. Nature *584*, 437–442.
18. Ibarrondo, F.J., Fulcher, J.A., Goodman-Meza, D., Elliott, J., Hofmann, C., Hausner, M.A., Ferbas, K.G., Tobin, N.H., Aldrovandi, G.M., and Yang, O.O. (2020). Rapid decay of anti-SARS-CoV-2 antibodies in persons with mild Covid-19. N. Engl. J. Med. *383*, 1085–1087.
19. Seow, J., Graham, C., Merrick, B., Acors, S., Pickering, S., Steel, K.J.A., Hemmings, O., O'Byrne, A., Kouphou, N., Galao, R.P., et al. (2020). Longitudinal observation and decline of neutralizing antibody responses in the three months following SARS-CoV-2 infection in humans. Nat. Microbiol. *5*, 1598–1607.
20. Pradenas, E., Trinité, B., Urrea, V., Marfil, S., Ávila-Nieto, C., Rodríguez de la Concepción, M.L., Tarrés-Freixas, F., Pérez-Yanes, S., Rovirosa, C., Ainsua-Enrich, E., et al. (2021). Stable neutralizing antibody levels 6 months after mild and severe COVID-19 episodes. Med (N Y) *2*, 313–320.e4.
21. Chan, C.E.Z., Seah, S.G.K., Chye, D.H., Massey, S., Torres, M., Lim, A.P.C., Wong, S.K.K., Neo, J.J.Y., Wong, P.S., Lim, J.H., et al. (2020). The Fc-mediated effector functions of a potent SARS-CoV-2 neutralizing antibody, SC31, isolated from an early convalescent COVID-19 patient, are essential for the optimal therapeutic efficacy of the antibody. bioRxiv. https://doi.org/10.1101/2020.10.26.355107.
22. Dufloo, J., Grzelak, L., Staropoli, I., Madec, Y., Tondeur, L., Anna, F., Pelleau, S., Wiedemann, A., Planchais, C., Buchrieser, J., et al. (2021). Asymptomatic and symptomatic SARS-CoV-2 infections elicit polyfunctional antibodies. Cell Rep. Med. Published online April 20, 2021. https://doi.org/10.1016/j.xcrm.2021.100275.p.
23. Zohar, T., Loos, C., Fischinger, S., Atyeo, C., Wang, C., Slein, M.D., Burke, J., Yu, J., Feldman, J., Hauser, B.M., et al. (2020). Compromised humoral functional evolution tracks with SARS-CoV-2 mortality. Cell *183*, 1508–1519.e12.
24. Anand, S.P., Prévost, J., Richard, J., Perreault, J., Tremblay, T., Drouin, M., Fournier, M.J., Lewin, A., Bazin, R., and Finzi, A. (2021). High-throughput detection of antibodies targeting the SARS-CoV-2 Spike in longitudinal convalescent plasma samples. Transfusion, Published online February 18, 2021. https://doi.org/10.1111/trf.16318.
25. Hansen, J., Baum, A., Pascal, K.E., Russo, V., Giordano, S., Wloga, E., Fulton, B.O., Yan, Y., Koon, K., Patel, K., et al. (2020). Studies in humanized mice and convalescent humans yield a SARS-CoV-2 antibody cocktail. Science *369*, 1010–1014.
26. Rogers, T.F., Zhao, F., Huang, D., Beutler, N., Burns, A., He, W.T., Limbo, O., Smith, C., Song, G., Woehl, J., et al. (2020). Isolation of potent SARS-CoV-2 neutralizing antibodies and protection from disease in a small animal model. Science *369*, 956–963.
27. Rojas, M., Rodríguez, Y., Monsalve, D.M., Acosta-Ampudia, Y., Camacho, B., Gallo, J.E., Rojas-Villarraga, A., Ramírez-Santana, C., Díaz-Coronado, J.C., Manrique, R., et al. (2020). Convalescent plasma in Covid-19: Possible mechanisms of action. Autoimmun. Rev. *19*, 102554.
28. Li, L., Zhang, W., Hu, Y., Tong, X., Zheng, S., Yang, J., Kong, Y., Ren, L., Wei, Q., Mei, H., et al. (2020). Effect of convalescent plasma therapy on time to clinical improvement in patients with severe and life-threatening COVID-19: a randomized clinical trial. JAMA *324*, 460–470.
29. Devasenapathy, N., Ye, Z., Loeb, M., Fang, F., Najafabadi, B.T., Xiao, Y., Couban, R., Bégin, P., and Guyatt, G. (2020). Efficacy and safety of convalescent plasma for severe COVID-19 based on evidence in other severe

respiratory viral infections: a systematic review and meta-analysis. CMAJ *192*, E745–E755.

30. Klingler, J., Weiss, S., Itri, V., Liu, X., Oguntuyo, K.Y., Stevens, C., Ikegame, S., Hung, C.-T., Enyindah-Asonye, G., Amanat, F., et al. (2020). Role of IgM and IgA antibodies in the neutralization of SARS-CoV-2. medRxiv. https://doi.org/10.1101/2020.08.18.20177303.
31. Gasser, R., Cloutier, M., Prévost, J., Fink, C., Ducas, É., Ding, S., Dussault, N., Landry, P., Tremblay, T., Laforce-Lavoie, A., et al. (2021). Major role of IgM in the neutralizing activity of convalescent plasma against SARS-CoV-2. Cell Rep. *34*, 108790.
32. Sterlin, D., Mathian, A., Miyara, M., Mohr, A., Anna, F., Claër, L., Quentric, P., Fadlallah, J., Devilliers, H., Ghillani, P., et al. (2021). IgA dominates the early neutralizing antibody response to SARS-CoV-2. Sci. Transl. Med. *13*, eabd2223.
33. Wang, Z., Lorenzi, J.C.C., Muecksch, F., Finkin, S., Viant, C., Gaebler, C., Cipolla, M., Hoffmann, H.H., Oliveira, T.Y., Oren, D.A., et al. (2021). Enhanced SARS-CoV-2 neutralization by dimeric IgA. Sci. Transl. Med. *13*, eabf1555.
34. Schäfer, A., Muecksch, F., Lorenzi, J.C.C., Leist, S.R., Cipolla, M., Bournazos, S., Schmidt, F., Maison, R.M., Gazumyan, A., Martinez, D.R., et al. (2021). Antibody potency, effector function, and combinations in protection and therapy for SARS-CoV-2 infection in vivo. J. Exp. Med. *218*, e20201993.
35. Tso, F.Y., Lidenge, S.J., Poppe, L.K., Peña, P.B., Privatt, S.R., Bennett, S.J., Ngowi, J.R., Mwaiselage, J., Belshan, M., Siedlik, J.A., et al. (2021). Presence of antibody-dependent cellular cytotoxicity (ADCC) against SARS-CoV-2 in COVID-19 plasma. PLoS ONE *16*, e0247640.
36. Song, G., He, W.T., Callaghan, S., Anzanello, F., Huang, D., Ricketts, J., Torres, J.L., Beutler, N., Peng, L., Vargas, S., et al. (2020). Cross-reactive serum and memory B cell responses to spike protein in SARS-CoV-2 and endemic coronavirus infection. bioRxiv. https://doi.org/10.1101/2020.09.22.308965.
37. Chen, X., Pan, Z., Yue, S., Yu, F., Zhang, J., Yang, Y., Li, R., Liu, B., Yang, X., Gao, L., et al. (2020). Disease severity dictates SARS-CoV-2-specific neutralizing antibody responses in COVID-19. Signal Transduct. Target. Ther. *5*, 180.
38. Huang, A.T., Garcia-Carreras, B., Hitchings, M.D.T., Yang, B., Katzelnick, L.C., Rattigan, S.M., Borgert, B.A., Moreno, C.A., Solomon, B.D., Trimmer-Smith, L., et al. (2020). A systematic review of antibody mediated immunity to coronaviruses: kinetics, correlates of protection, and association with severity. Nat. Commun. *11*, 4704.
39. Abu-Raddad, L.J., Chemaitelly, H., Coyle, P., Malek, J.A., Ahmed, A.A., Mohamoud, Y.A., Younuskunju, S., Ayoub, H.H., Al Kanaani, Z., Al Kuwari, E., et al. (2021). SARS-CoV-2 reinfection in a cohort of 43,000 antibody-positive individuals followed for up to 35 weeks. medRxiv. https://doi.org/10.1101/2021.01.15.21249731.
40. Natarajan, H., Crowley, A.R., Butler, S.E., Xu, S., Weiner, J.A., Bloch, E.M., Littlefield, K., Wieland-Alter, W., Connor, R.I., Wright, P.F., et al. (2020). SARS-CoV-2 antibody signatures robustly predict diverse antiviral functions relevant for convalescent plasma therapy. medRxiv. https://doi.org/10.1101/2020.09.16.20196154.
41. Wang, Z., Schmidt, F., Weisblum, Y., Muecksch, F., Barnes, C.O., Finkin, S., Schaefer-Babajew, D., Cipolla, M., Gaebler, C., Lieberman, J.A., et al. (2021). mRNA vaccine-elicited antibodies to SARS-CoV-2 and circulating variants. Nature *592*, 616–622.
42. Ullah, I., Prévost, J., Ladinsky, M.S., Stone, H., Lu, M., Anand, S.P., Beaudoin-Bussières, G., Benlarbi, M., Ding, S., Gasser, R., et al. (2021). Live imaging of SARS-CoV-2 infection in mice reveals neutralizing antibodies require Fc function for optimal efficacy. bioRxiv. https://doi.org/10.1101/2021.03.22.436337.
43. Brunet-Ratnasingham, E., Anand, S.P., Gantner, P., Moquin-Beaudry, G., Dyachenko, A., Brassard, N., Beaudoin-Bussières, G., Pagliuzza, A., Gasser, R., Benlarbi, M., et al. (2021). Integrated immunovirological profiling validates plasma SARS-CoV-2 RNA as an early predictor of COVID-19 mortality. medRxiv. https://doi.org/10.1101/2021.03.18.21253907.
44. ter Meulen, J., van den Brink, E.N., Poon, L.L., Marissen, W.E., Leung, C.S., Cox, F., Cheung, C.Y., Bakker, A.Q., Bogaards, J.A., van Deventer, E., et al. (2006). Human monoclonal antibody combination against SARS coronavirus: synergy and coverage of escape mutants. PLoS Med. *3*, e237.
45. Liu, Z., Pan, Q., Ding, S., Qian, J., Xu, F., Zhou, J., Cen, S., Guo, F., and Liang, C. (2013). The interferon-inducible MxB protein inhibits HIV-1 infection. Cell Host Microbe *14*, 398–410.
46. Lodge, R., Lalonde, J.P., Lemay, G., and Cohen, E.A. (1997). The membrane-proximal intracytoplasmic tyrosine residue of HIV-1 envelope glycoprotein is critical for basolateral targeting of viral budding in MDCK cells. EMBO J. *16*, 695–705.
47. R Studio Team (2015). RStudio: Integrated Development for R (RStudio).
48. R Development Core Team (2013). R: A language and environment for statistical computing (R Foundation for Statistical Computing).
49. Mauri, M., Elli, T., Caviglia, G., Uboldi, G., and Azzi, M. (2017). RAWGraphs: a visualisation platform to create open outputs. In Proceedings of the 12th Biannual Conference on Italian SIGCHI Chapter (Association for Computing Machinery).

STAR★METHODS

KEY RESOURCES TABLE

REAGENT or RESOURCE	SOURCE	IDENTIFIER
Antibodies		
Cross-reactive SARS-CoV-1 monoclonal antibody CR3022	ter Meulen et al.[44]	RRID: AB_2848080
Alexa Fluor 647 AffiniPure Goat Anti-Human IgA + IgG + IgM (H+L)	Jackson ImmunoResearch	Cat# 109-605-064; RRID: AB_2337886
Goat anti-Human IgG Fc Cross-Adsorbed Secondary Antibody, HRP	Invitrogen	Cat# A18823; RRID: AB_2535600
Peroxidase AffiniPure Goat Anti-Human IgM, Fc5μ fragment specific	Jackson ImmunoResearch	Cat# 109-035-129; RRID: AB_2337588
Peroxidase AffiniPure Goat Anti-Human Serum IgA, α chain specific	Jackson ImmunoResearch	Cat# 109-035-011; RRID: AB_2337580
Peroxidase AffiniPure Goat Anti-Human IgA + IgG + IgM (H+L)	Jackson ImmunoResearch	Cat# 109-035-064; RRID: AB_2337583
BUV805 Mouse Anti-Human CD24 (Clone ML5)	BD Biosciences	Cat# 742010; RRID: AB_2871308
BV421 Mouse Anti-Human IgG (Clone G18-145)	BD Biosciences	Cat# 562581; RRID: AB_2737665
BUV737 Mouse Anti-Human IgM (Clone UCH-B1)	BD Biosciences	Cat# 748928; RRID: AB_2873331
BV480 Mouse Anti-Human CD3 (Clone UCHT1)	BD Biosciences	Cat# 566105, RRID: AB_2739507
BV480 Mouse Anti-Human CD56 (Clone NCAM16.2)	BD Biosciences	Cat# 566124; RRID: AB_2739525
BV480 Mouse Anti-Human CD14 (Clone M5E2)	BD Biosciences	Cat# 746304; RRID: AB_2743629
BV480 Mouse Anti-Human CD16 (Clone 3G8)	BD Biosciences	Cat# 566171; RRID: AB_2739510
BV711 Mouse Anti-Human CD20 (Clone 2H7)	BD Biosciences	Cat# 563126; RRID: AB_2313579
BV786 Mouse Anti-Human CD21 (Clone B-ly4)	BD Biosciences	Cat# 740969; RRID: AB_2740594
BB700 Mouse Anti-Human HLA-DR (Clone G46-6)	BD Biosciences	Cat# 566480; RRID: AB_2744477
APC-R700 Mouse Anti-Human CD27 (Clone M-T271)	BD Biosciences	Cat# 565116; RRID: AB_2739074
APC anti-human CD19 (Clone SJ25C1)	BioLegend	Cat# 363006; RRID: AB_2564255
PE Mouse Anti-Human IgA (Clone IS11-8E10)	Miltenyi Biotec	Cat# 130-113-476; RRID: AB_2733861
Biological samples		
Human Plasma from SARS-CoV-2-infected or uninfected donors	This paper	N/A
Peripheral blood mononuclear cells (PBMCs) from SARS-CoV-2 infected donors or uninfected donors	This paper	N/A
Chemicals, peptides, and recombinant proteins		
Dulbecco's modified Eagle's medium (DMEM)	Wisent	Cat# 319-005-CL
Roswell Park Memorial Institute 1640 medium (RPMI)	GIBCO Life Technologies	Cat# 11875093
Penicillin/streptomycin	Wisent	Cat# 450-201-EL
Penicillin/streptomycin	GIBCO Life Technologies	Cat# 15140122
Fetal bovine serum (FBS)	VWR	Cat# 97068-085
Fetal bovine serum (FBS)	Seradigm	Cat# 1500-500
Tris-buffered saline (TBS)	Thermo Fisher Scientific	Cat# BP24711
Bovine Serum Albumin (BSA)	BioShop	Cat# ALB001.100
Phosphate buffered saline (PBS)	Wisent	Cat# 311-010-CL
Dulbecco's phosphate-buffered saline (DPBS)	GIBCO Life Technologies	Cat# 14190144
Western Lightning Plus-ECL, Enhanced Chemiluminescence Substrate	Perkin Elmer Life Sciences	Cat# NEL105001EA
Tween20	Thermo Fisher Scientific	Cat# BP337-500
Puromycin dihydrochloride	Millipore Sigma	Cat# P8833
Passive lysis buffer	Promega	Cat# E1941

(*Continued on next page*)

Continued

REAGENT or RESOURCE	SOURCE	IDENTIFIER
FreeStyle 293F expression medium	ThermoFisher Scientific	Cat# 12338002
ExpiFectamine 293 transfection reagent	ThermoFisher Scientific	Cat# A14525
Ni-NTA agarose	Invitrogen	Cat# R90110
D-Luciferin potassium salt	Thermo Fisher Scientific	Cat# L2916
LIVE/DEAD Fixable AquaVivid Cell Stain	Thermo Fisher Scientific	Cat# L34957
Formaldehyde 37%	Thermo Fisher Scientific	Cat# F79-500
HEPES (1 M)	GIBCO Life Technologies	Cat# 15630080
Skim milk (non fat powder)	BioShop	Cat# SKI400.1
eBioscience Cell Proliferation Dye eFluor 670	ThermoFisher Scientific	Cat# 65-0840-85
eBioscience Cell Proliferation Dye eFluor 450	ThermoFisher Scientific	Cat# 65-0842-85
Critical commercial assays		
Alexa Fluor 594 Protein Labeling Kit	Invitrogen	Cat# A10239
Alexa Fluor 488 Protein Labeling Kit	Invitrogen	Cat# A10235
Experimental models: Cell lines		
HEK293T human embryonic kidney cells	ATCC	Cat# CRL-3216; RRID: CVCL_0063
FreeStyle 293F	ThermoFisher Scientific	Cat# R79007; RRID: CVCL_D603
293T-ACE2	Prévost et al.[16]	N/A
293T-Spike	Anand et al.[24]	N/A
Human osteosarcoma (HOS)	ATCC	Cat# CRL-1543; RRID: CVCL_0312
HOS-Spike	This paper	N/A
CEM.NKr CCR5+	NIH AIDS Reagent Program	Cat # 4376; RRID: CVCL_X623
CEM.NKr-Spike	This paper	N/A
Recombinant DNA		
pNL4.3 R-E- Luc	NIH AIDS Reagent Program	Cat# 3418
pCG1-SARS-CoV-2 Spike	Hoffmann et al.[13]	N/A
Lentiviral packaging plasmids (pLP1, pLP2)	Liu et al.[45]	N/A
pSVCMV-IN-VSV-G	Lodge et al.[46]	N/A
pLV-SARS-CoV-2 S C-GFPSpark tag	Sino Biological	Cat# VG40590-ACGLN
pcDNA3.1(+)-SARS-CoV-2 RBD	Beaudoin-Bussières et al.[14]	N/A
Software and algorithms		
FlowJo v10	Tree Star	https://www.flowjo.com/
GraphPad Prism v9	GraphPad	https://www.graphpad.com/
R v3	R	https://www.r-project.org/
RStudio v1	RStudio	https://www.rstudio.com/
Microsoft Excel v16	Microsoft Office	https://www.microsoft.com/en-ca/microsoft-365/excel
Other		
BD LSR II Flow Cytometer	BD Biosciences	N/A
TriStar LB 942 Microplate Reader	Berthold Technologies	N/A

RESOURCE AVAILABILITY

Lead contact

Further information and requests for resources and reagents should be directed to and will be fulfilled by the lead contact, Andrés Finzi (andres.finzi@umontreal.ca).

Materials availability

All unique reagents generated in this study are available from the lead contact with a completed Materials Transfer Agreement.

Data and code availability

All data are included in the manuscript. This study did not generate new or custom code.

EXPERIMENTAL MODEL AND SUBJECT DETAILS

Ethics Statement

All work was conducted in accordance with the Declaration of Helsinki in terms of informed consent and approval by an appropriate institutional board. Convalescent plasmas were obtained from donors who consented to participate in this research project at CHUM (19.381). The donors met all donor eligibility criteria: previous confirmed COVID-19 infection and complete resolution of symptoms for at least 14 days.

Human subjects

The present study aims to determine the kinetics of the humoral response following SARS-CoV-2 infection. All available samples from adults recovered from SARS-CoV-2 infection collected at the time of the study were analyzed. No specific criteria such as number of patients (sample size), clinical or demographic were used for inclusion, beyond PCR confirmed SARS-CoV-2 infection in adults. A summary of demographic parameters for all individuals is included in Table 1. While all the participants were symptomatic at the time of the infection, none of them were hospitalized. The disease severity ranged from mild to moderate symptoms without any severe or critical cases.

Cell lines

293T human embryonic kidney cells and HOS cells (obtained from ATCC) were maintained at 37°C under 5% CO_2 in Dulbecco's modified Eagle's medium (DMEM) (Wisent) containing 5% fetal bovine serum (VWR) and 100 μg/ml penicillin-streptomycin (Wisent). CEM.NKr CCR5+ cells (NIH AIDS Reagent Program) were maintained at 37°C under 5% CO_2 in RPMI (GIBCO) containing 10% fetal bovine serum (VWR) and 100 μg/ml penicillin-streptomycin (Wisent). 293T-ACE2 and 293T-SARS-CoV-2 Spike cell lines were previously reported[16]. For the generation of HOS and CEM.NKr CCR5+ cells stably expressing the SARS-CoV-2 Spike glycoproteins, transgenic lentiviruses were produced in 293T using a third-generation lentiviral vector system. Briefly, 293T cells were co-transfected with two packaging plasmids (pLP1 and pLP2[45]), an envelope plasmid (pSVCMV-IN-VSV-G[46]) and a lentiviral transfer plasmid coding for a GFP-tagged SARS-CoV-2 Spike (pLV-SARS-CoV-2 S C-GFPSpark tag) (Sino Biological). Supernatant containing lentiviral particles was used to transduce HOS and CEM.NKr CCR5+ cells in presence of 5 μg/mL polybrene. The HOS and CEM.NKr CCR5+ cells stably expressing SARS-CoV-2 Spike (GFP+) were sorted by flow cytometry.

METHOD DETAILS

Plasma and antibodies

Plasma from SARS-CoV-2-infected and pre-pandemic uninfected donors were collected, heat-inactivated for 1h at 56°C and stored at −80°C until ready to use in subsequent experiments. Plasma from uninfected donors were used as negative controls and used to calculate the seropositivity threshold in our ELISA, cell-based ELISA, and flow cytometry assays. The RBD-specific monoclonal antibody CR3022[44] was used as a positive control in our ELISAs, cell-based ELISAs, and flow cytometry assays and was previously described[14,16,24]. Horseradish peroxidase (HRP)-conjugated antibodies able to detect all Ig isotypes (anti-human IgM+IgG+IgA; Jackson ImmunoResearch Laboratories, Inc.) or specific for the Fc region of human IgG (Invitrogen), the Fc region of human IgM (Jackson ImmunoResearch Laboratories, inc.) or the Fc region of human IgA (Jackson ImmunoResearch Laboratories, inc) were used as secondary antibodies to detect antibody binding in ELISA and cell-based ELISA experiments. Alexa Fluor-647-conjugated goat anti-human Abs able to detect all Ig isotypes (anti-human IgM+IgG+IgA; Jackson ImmunoResearch Laboratories, Inc.) were used as secondary antibodies to detect plasma binding in flow cytometry experiments.

Protein expression and purification

FreeStyle 293F cells (Thermo Fisher Scientific) were grown in FreeStyle 293F medium (Thermo Fisher Scientific) to a density of 1×10^6 cells/mL at 37°C with 8% CO_2 with regular agitation (150 rpm). Cells were transfected with a plasmid coding for SARS-CoV-2 S RBD using ExpiFectamine 293 transfection reagent, as directed by the manufacturer (Thermo Fisher Scientific). One week later, cells were pelleted and discarded. Supernatants were filtered using a 0.22 μm filter (Thermo Fisher Scientific). The recombinant RBD proteins were purified by nickel affinity columns, as directed by the manufacturer (Invitrogen). The RBD preparations were dialyzed against phosphate-buffered saline (PBS) and stored in aliquots at −80°C until further use. To assess purity, recombinant proteins were loaded on SDS-PAGE gels and stained with Coomassie Blue.

Enzyme-Linked Immunosorbent Assay (ELISA)

The SARS-CoV-2 RBD ELISA assay used was recently described[16]. Briefly, recombinant SARS-CoV-2 S RBD proteins (2.5 μg/ml), or bovine serum albumin (BSA) (2.5 μg/ml) as a negative control, were prepared in PBS and adsorbed to plates (MaxiSorp Nunc) overnight at 4°C. Coated wells were subsequently blocked with blocking buffer (Tris-buffered saline [TBS] containing 0.1% Tween20

and 2% BSA) for 1h at room temperature. Wells were then washed four times with washing buffer (Tris-buffered saline [TBS] containing 0.1% Tween20). CR3022 mAb (50ng/ml) or a 1/250 dilution of plasma from SARS-CoV-2-infected or uninfected donors were prepared in a diluted solution of blocking buffer (0.1% BSA) and incubated with the RBD-coated wells for 90 minutes at room temperature. Plates were washed four times with washing buffer followed by incubation with the respective secondary Abs (diluted in blocking buffer, 0.4% BSA) for 1h at room temperature. The binding of CR3022 IgG was quantified with HRP-conjugated antibodies specific for the Fc region of human IgG. This was followed by four washes. HRP enzyme activity was determined after the addition of a 1:1 mix of Western Lightning oxidizing and luminol reagents (Perkin Elmer Life Sciences). Light emission was measured with a LB942 TriStar luminometer (Berthold Technologies). Signal obtained with BSA was subtracted for each plasma and was then normalized to the signal obtained with CR3022 mAb present in each plate. The seropositivity threshold was established using the following formula: mean of all COVID-19 negative plasma + (3 standard deviation of the mean of all COVID-19 negative plasma).

Cell-Based ELISA

Detection of the trimeric SARS-CoV-2 Spike at the surface of HOS cells was performed by cell-based enzyme-linked immunosorbent assay (ELISA). Briefly, parental HOS cells or HOS-Spike cells were seeded in 384-well plates (2.8×10^4 cells per well) overnight. Cells were blocked with blocking buffer (washing buffer [1.8 mM $CaCl_2$, 1 mM $MgCl_2$, 25 mM Tris (pH 7.5), and 140 mM NaCl] supplemented with 10mg/mL non-fat dry milk and 5mM Tris [pH 8.0]) for 30min. CR3022 mAb (1 μg/ml) or plasma from SARS-CoV-2-infected or uninfected donors (at a dilution of 1/250) were prepared in blocking buffer and incubated with the cells for 1h at room temperature. Respective HRP-conjugated secondary antibodies were then incubated with the samples for 45 min at room temperature. The binding of CR3022 IgG was quantified with HRP-conjugated antibodies specific for the Fc region of human IgG. For all conditions, cells were washed 6 times with blocking buffer and 6 times with washing buffer. HRP enzyme activity was determined after the addition of a 1:1 mix of Western Lightning oxidizing and luminol reagents (PerkinElmer Life Sciences). Light emission was measured with an LB 942 TriStar luminometer (Berthold Technologies). Signal obtained with parental HOS was subtracted for each plasma and was then normalized to the signal obtained with CR3022 mAb present in each plate. The seropositivity threshold was established using the following formula: mean of all COVID-19 negative plasma + (3 standard deviation of the mean of all COVID-19 negative plasma).

Cell surface staining and flow cytometry analysis

293T and 293T-Spike cells were mixed at a 1:1 ratio and stained with the anti-RBD CR3022 monoclonal Ab (5 μg/ml) or plasma (1:250 dilution). AlexaFluor-647-conjugated goat anti-human IgM+IgG+IgA Abs (1:800 dilution) were used as secondary antibodies. The percentage of transduced cells (GFP+ cells) was determined by gating the living cell population based on viability dye staining (Aqua Vivid, Invitrogen). Samples were acquired on a LSRII cytometer (BD Biosciences) and data analysis was performed using FlowJo v10.7.1 (Tree Star). The seropositivity threshold was established using the following formula: mean of all COVID-19 negative plasma + (3 standard deviation of the mean of all COVID-19 negative plasma).

ADCC assay

For evaluation of anti-SARS-CoV-2 antibody-dependent cellular cytotoxicity (ADCC), parental CEM.NKr CCR5+ cells were mixed at a 1:1 ratio with CEM.NKr. Spike cells. These cells were stained for viability (AquaVivid; Thermo Fisher Scientific, Waltham, MA, USA) and cellular dyes (cell proliferation dye eFluor670; Thermo Fisher Scientific) and subsequently used as target cells. Overnight rested PBMCs were stained with another cellular marker (cell proliferation dye eFluor450; Thermo Fisher Scientific) and used as effector cells. Stained target and effector cells were mixed at a ratio of 1:10 in 96-well V-bottom plates. Plasma from COVID+ or COVID- individuals (1/500 dilution) or monoclonal antibody CR3022 (1 μg/mL) were added to the appropriate wells. The plates were subsequently centrifuged for 1 min at 300xg, and incubated at 37°C, 5% CO_2 for 5 hours before being fixed in a 2% PBS-formaldehyde solution. ADCC activity was calculated using the formula: [(% of GFP+ cells in Targets plus Effectors)-(% of GFP+ cells in Targets plus Effectors plus plasma/antibody)]/(% of GFP+ cells in Targets) x 100 by gating on transduced live target cells. All samples were acquired on an LSRII cytometer (BD Biosciences) and data analysis performed using FlowJo v10.7.1 (Tree Star). The specificity threshold was established using the following formula: mean of all COVID-19 negative plasma + (3 standard deviation of the mean of all COVID-19 negative plasma)

Virus neutralization assay

293T-ACE2 target cells were infected with single-round luciferase-expressing SARS-CoV-2 pseudoparticles in presence of convalescent plasma. Briefly, 293T cells were transfected by the calcium phosphate method with the lentiviral vector pNL4.3 R-E- Luc (NIH AIDS Reagent Program) and a plasmid encoding for SARS-CoV-2 Spike at a ratio of 5:4. Two days post-transfection, cell supernatants were harvested and stored at −80°C until use. 293T-ACE2 target cells were seeded at a density of 1×10^4 cells/well in 96-well luminometer-compatible tissue culture plates (Perkin Elmer) 24h before infection. Recombinant viruses in a final volume of 100 μL were incubated with the indicated plasma dilutions (1/50; 1/250; 1/1250; 1/6250; 1/31250) for 1h at 37°C and were then added to the target cells followed by incubation for 48h at 37°C; cells were lysed by the addition of 30 μL of passive lysis buffer (Promega) followed by one freeze-thaw cycle. An LB942 TriStar luminometer (Berthold Technologies) was used to measure the luciferase activity of each well after the addition of 100 μL of luciferin buffer (15mM $MgSO_4$, 15mM KPO_4 [pH 7.8], 1mM ATP, and 1mM

dithiothreitol) and 50 μL of 1mM d-luciferin potassium salt (Thermo Fisher Scientific). The neutralization half-maximal inhibitory dilution (ID_{50}) represents the plasma dilution to inhibit 50% of the infection of 293T-ACE2 cells by SARS-CoV-2 pseudoviruses.

Detection of antigen-specific B cells

To detect SARS-CoV-2-specific B cells, we conjugated recombinant RBD proteins with Alexa Fluor 488 or Alexa Fluor 594 (Thermo Fisher Scientific) according to the manufacturer's protocol. Approximately 10×10^6 frozen PBMC from 13 convalescent donors were prepared in Falcon® 5ml-round bottom polystyrene tubes at a final concentration of 14×10^6 cells/mL in RPMI 1640 medium (GIBCO) supplemented with 10% of fetal bovine serum (Seradigm), Penicillin- Streptomycin (GIBCO) and HEPES (GIBCO). After a rest of 2h at 37°C and 5% CO_2, cells were stained using Aquavivid viability marker (GIBCO) in DPBS (GIBCO) at 4°C for 20min. The detection of SARS-CoV-2-antigen specific B cells was done by adding the RBD probes to the following antibody cocktail: IgM BUV737, CD24 BUV805, IgG BV421, CD3 BV480, CD56 BV480, CD14 BV480, CD16 BV480, CD20 BV711, CD21 BV786, HLA DR BB700, CD27 APC R700 all from BD Biosciences; CD19 BV650 from Biolegend and IgA PE from Miltenyi. Staining was performed at 4°C for 30min and cells were fixed using 2% paraformaldehyde at 4°C for 15min. Stained PBMC samples were acquired on Symphony cytometer (BD Biosciences) and analyzed using FlowJo v10.7.1 (TreeStar). In each experiment, PBMC from unexposed donors (total of n = 9) were included to ensure consistent specificity of the assay.

QUANTIFICATION AND STATISTICAL ANALYSIS

Statistical analyses

Statistics were analyzed using GraphPad Prism version 9.0.0 (GraphPad, San Diego, CA). Every dataset was tested for statistical normality and this information was used to apply the appropriate (parametric or nonparametric) statistical test. P values < 0.05 were considered significant; significance values are indicated as * $p < 0.05$, ** $p < 0.01$, *** $p < 0.001$, **** $p < 0.0001$. Multiplicity adjustments of p values were performed with the Benjamini-Hochberg method in R and R Studio[47,48] using the data.table and tidyverse packages.

Software scripts and visualization

Normalized heatmaps were generated using the complexheatmap, tidyverse, and viridis packages in R and RStudio[47,48]. Normalizations were done per parameter. IDs were grouped and clustered separately according to time point. Correlograms were generated using the corrplot and RColorBrewer packages in program R and RStudio using hierarchical clustering according to the first principal component (FPC). Circular barplots were generated in R and RStudio using the tidyverse package with averaged, normalized data per parameter and time point. Edge bundling graphs were generated in undirected mode in R and RStudio using ggraph, igraph, tidyverse, and RColorBrewer packages. Edges are only shown if $p < 0.05$, and nodes are sized according to the connecting edges' r values. Nodes are color-coded according to groups of parameters. Area graphs were generated for the display of normalized time series. The plots were created in RawGraphs using DensityDesign interpolation and vertically un-centered values[49].

Cell Reports Medicine, Volume *2*

Supplemental information

Longitudinal analysis of humoral immunity against SARS-CoV-2 Spike in convalescent individuals up to 8 months post-symptom onset

Sai Priya Anand, Jérémie Prévost, Manon Nayrac, Guillaume Beaudoin-Bussières, Mehdi Benlarbi, Romain Gasser, Nathalie Brassard, Annemarie Laumaea, Shang Yu Gong, Catherine Bourassa, Elsa Brunet-Ratnasingham, Halima Medjahed, Gabrielle Gendron-Lepage, Guillaume Goyette, Laurie Gokool, Chantal Morrisseau, Philippe Bégin, Valérie Martel-Laferrière, Cécile Tremblay, Jonathan Richard, Renée Bazin, Ralf Duerr, Daniel E. Kaufmann, and Andrés Finzi

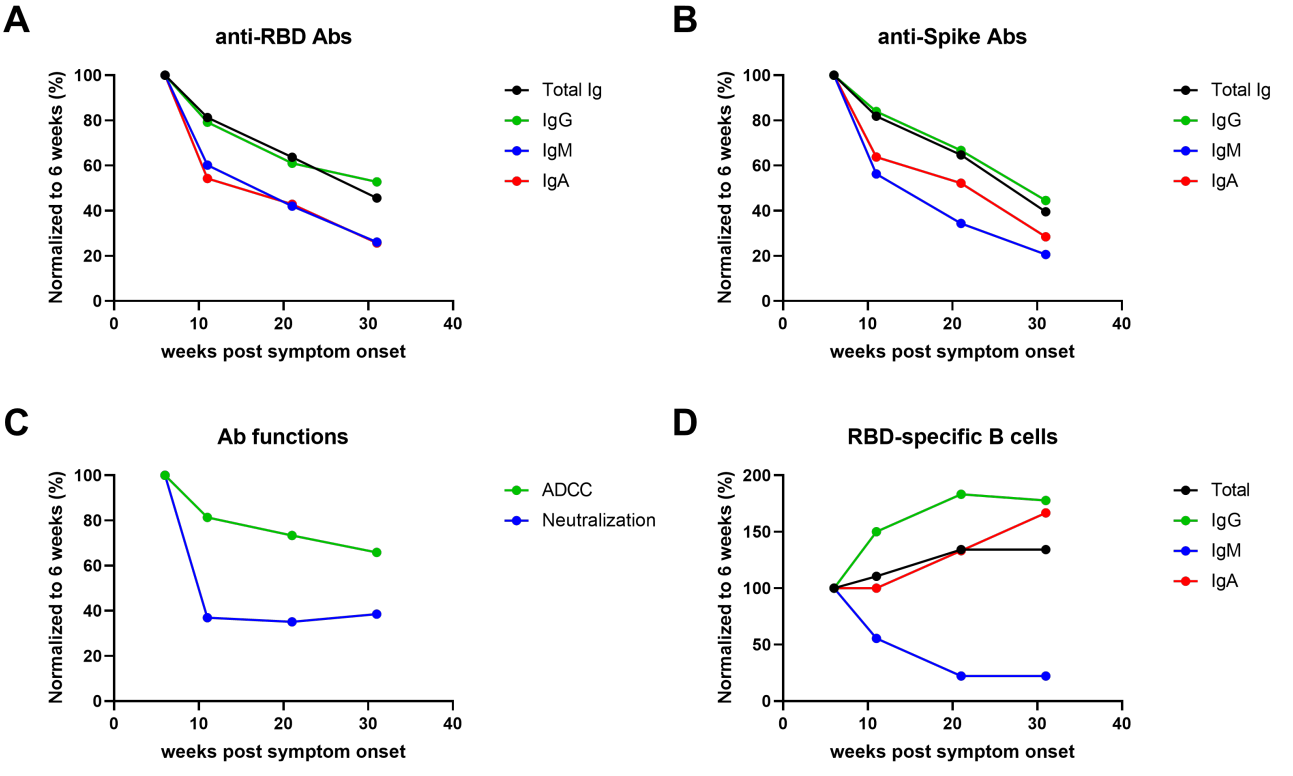

Supplemental Figure 1. Anti-SARS-CoV-2 IgM and IgA levels decline faster than IgG in the convalescence phase - Related to Figure 1, 2 & 3.

(A) The graph shown represents the mean values for anti-RBD ELISA (from Figure 1A-D) at different timepoints (6, 11, 21 and 31 weeks) normalized to the 6 weeks timepoint. (B) The graph shown represents the mean values for anti-Spike cell-based ELISA (from Figure 1E-H) at different timepoints (6, 11, 21 and 31 weeks) normalized to the 6 weeks timepoint. (C) The graph shown represents the mean values for neutralization and ADCC responses (from Figure 2) at different timepoints (6, 11, 21 and 31 weeks) normalized to the 6 weeks timepoint. (D) The graph shown represents the mean values for RBD-specific B cell frequencies (from Figure 3B-E) at different timepoints (6, 11, 21 and 31 weeks) normalized to the 6 weeks timepoint.

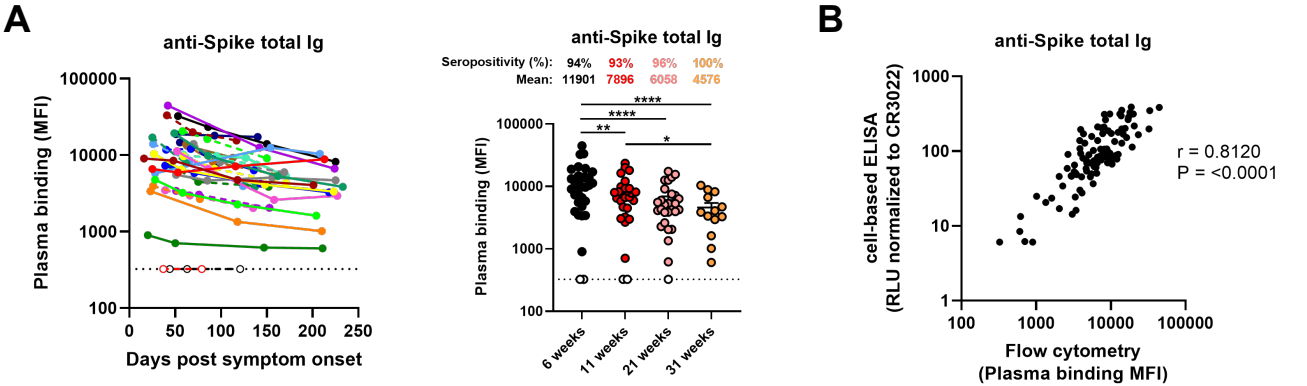

Supplemental Figure 2. Detection of antibodies against SARS-CoV-2 Spike by flow cytometry correlates with anti-Spike detection by cell-based ELISA - Related to Figure 1.

(A) Cell-surface staining of 293T cells stably expressing full-length SARS-CoV-2 Spike using samples from COVID-19+ convalescent donors at different times after symptoms onset (6, 11, 21 and 31 weeks). The graphs shown represent the median fluorescence intensities (MFI) obtained on the GFP+ population. MFIs values obtained with parental 293T (GFP-) were subtracted. (Left panel) Each curve represents the MFIs obtained with the plasma of one donor at every donation as a function of the days after symptom onset. (Right panel) Plasma samples were grouped in different timepoints post-symptom onset (6, 11, 21 and 31 weeks). Undetectable measures are represented as white symbols, and limits of detection are plotted. Error bars indicate means ± SEM. (B) The levels of anti-Spike total Ig quantified by flow cytometry were correlated with the level of anti-Spike total Ig quantified by cell-based ELISA. Statistical significance was tested using (A) a repeated measures one-way ANOVA with a Holm-Sidak post-test or (B) a Spearman correlation rank test (* $P < 0.05$; ** $P < 0.01$; **** $P < 0.0001$).

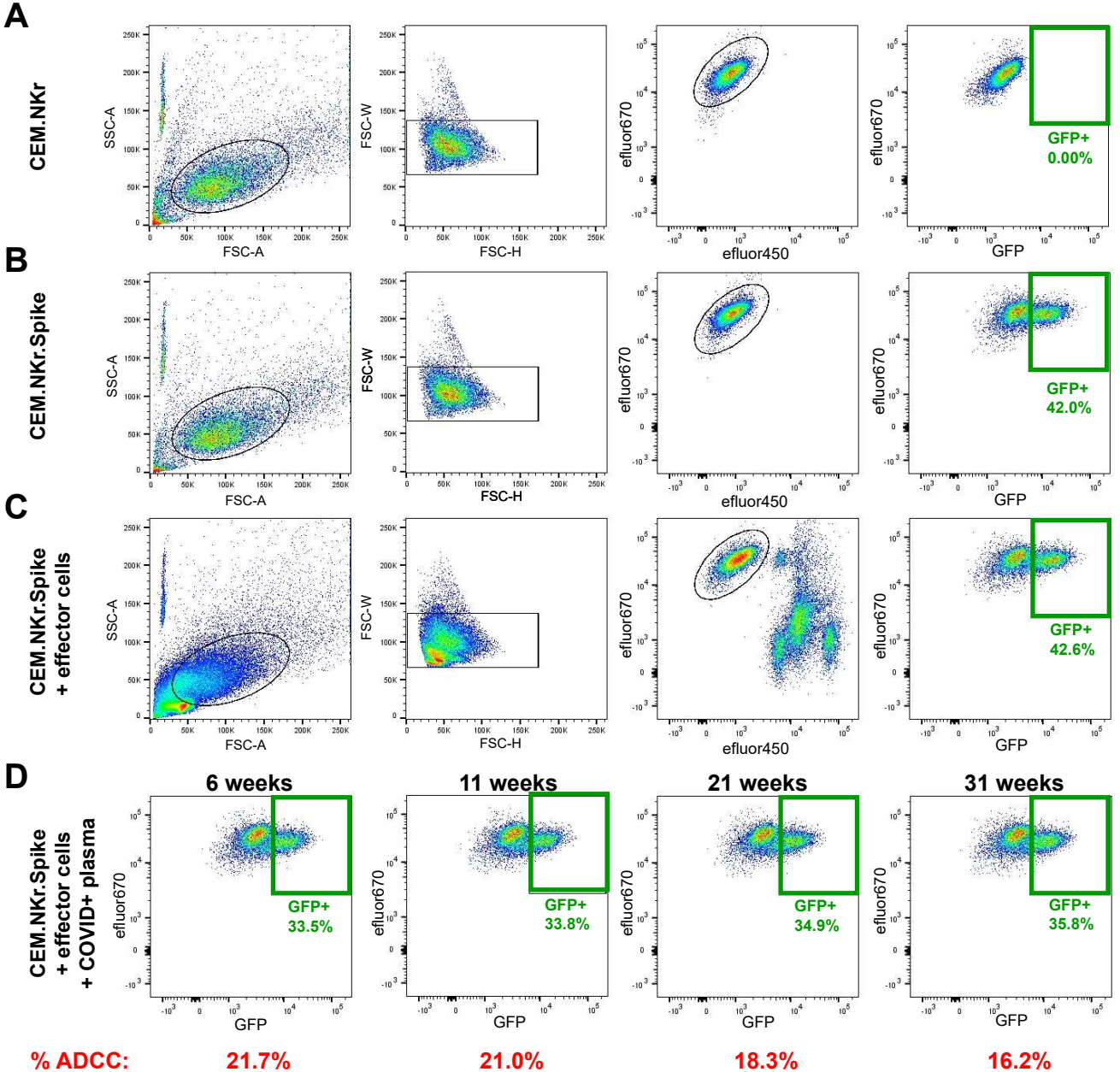

Supplemental Figure 3. Gating strategy for ADCC measurements - Related to Figure 2.
Target cells were identified according to cell morphology by light-scatter parameters (first column) and excluding doublets cells (second column). Cells were then gated on eFluor670+ cells (excluding the effector cells labeled with eFluor450; third column). Finally, the percentage of GFP+ target cells was used to calculate ADCC activity (last column). Examples of gating using (A) parental CEM.NKr or (B) a 1:1 ratio mix of CEM.NKr and CEM.NKr.Spike as target cells in absence or (C) in presence of effector cells. (D) ADCC assay performed in the presence of plasma samples from one representative convalescent donor at 4 different timepoints post-symptom onset (6, 11, 21 and 31 weeks).

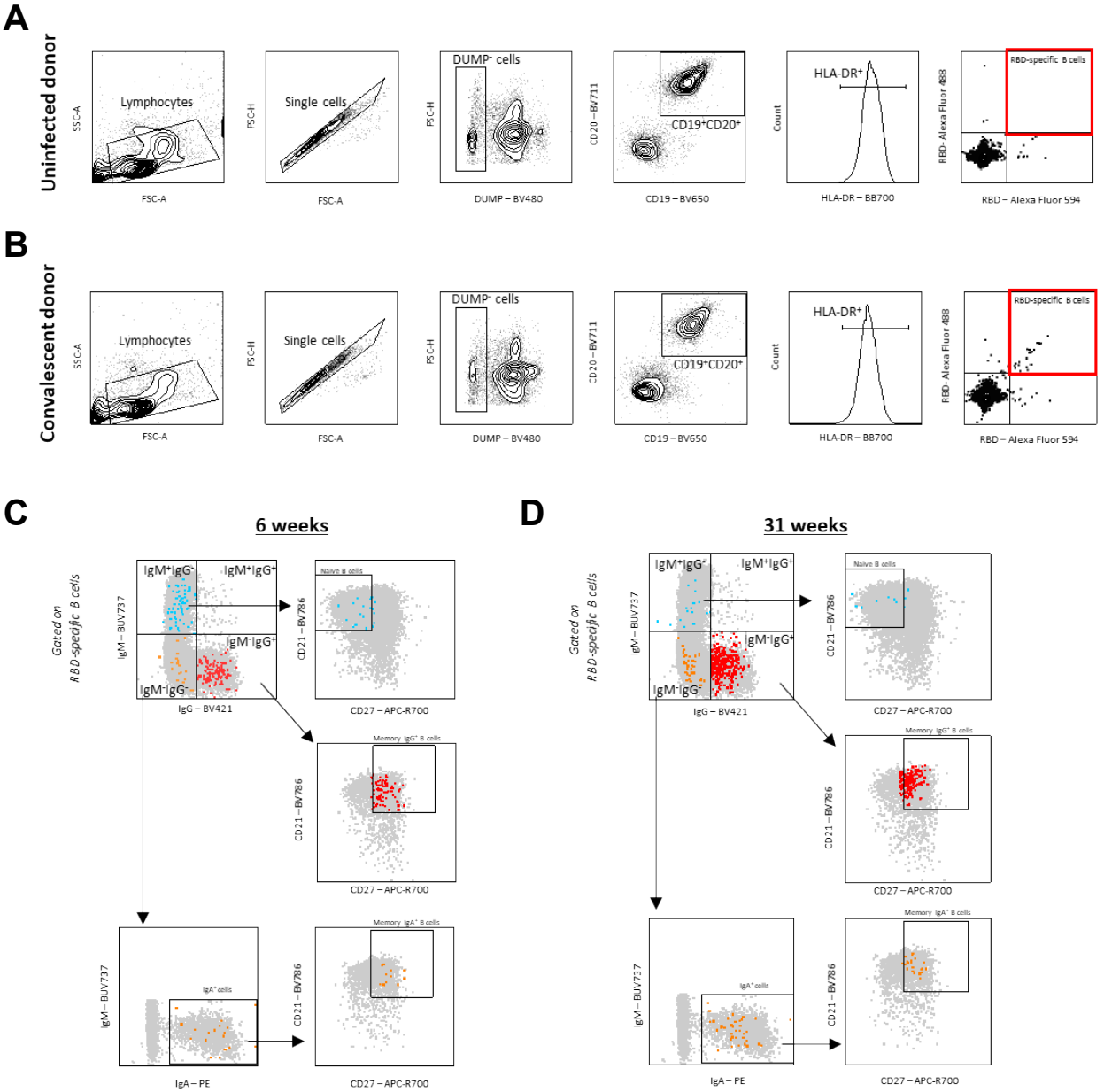

Supplemental Figure 4. Gating strategy for SARS-CoV-2-specific B cell characterization - Related to Figure 3. (A-B) Representative flow cytometry gates to identify RBD-specific B cells from PBMCs of (A) uninfected and (B) convalescent donor. (C-D) Flow cytometry gates used to differentiate RBD-specific B cell subtypes using isotypic and maturation cell surface markers on samples obtained (C) 6 weeks and (D) 31 weeks post-symptom onset. After identification of isotypic subtypes, RBD-specific naïve and memory B cells were characterized based on surface expression of CD21 and CD27. The different RBD-specific B cell subpopulations were superimposed on total CD19+/CD20+/HLA-DR+ B cells (grey). Legend: IgM+ and naïve IgM+ B cells, blue; IgG+ and memory IgG+ B cells, red; IgA+ and memory IgA+ B cells, orange.

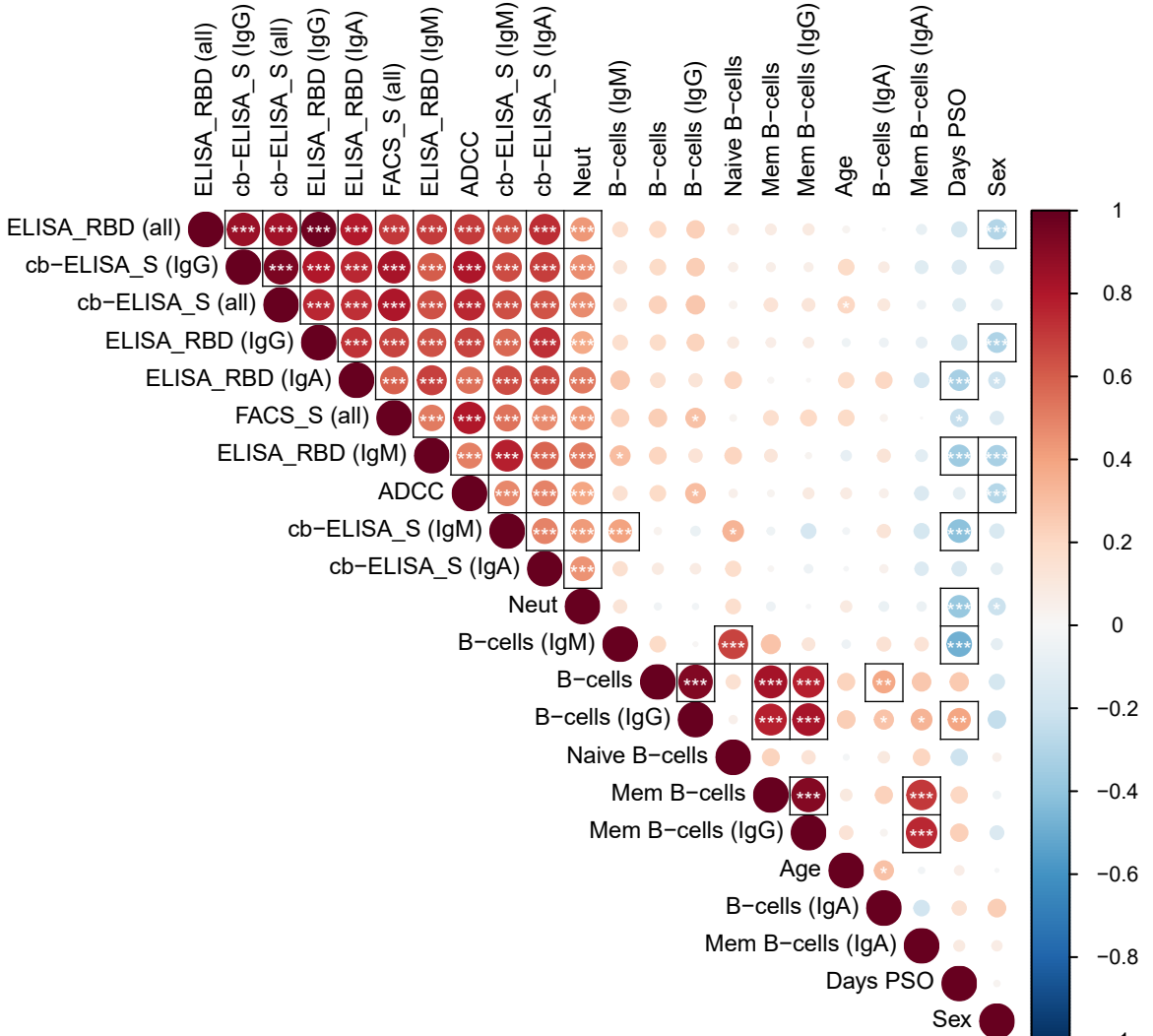

Supplemental Figure 5. Correlations between serological, immunological and demographic determinants - Related to Figure 5.

Correlograms were generated by plotting together all serological, immunological and demographic data obtained from convalescent patients. Circles are color-coded and sized according to the magnitude of the correlation coefficient (r). Red circles represent positive correlations between two variables and blue circles represent negative correlations. Asterisks indicate statistically significant correlations (*P < 0.05, **P < 0.01, ***P < 0.005). Correlation analysis was done using Spearman correlation rank tests. Parameters are clustered hierarchically according to the first principal component (FPC). Black surrounding boxes indicate adjusted p-values < 0.05 using Benjamini-Hochberg multiplicity correction. Legend: Cb-ELISA = cell-based ELISA, Neut = Neutralization, mem = memory, PSO =